Pharmaceutical Sciences and Drug Design
ISSN: 3062-4428
2025, Volume 5, Page No: 335-359
Copyright CC BY-NC-SA 4.0
Available online at: www.galaxypub.co/page/journals

Galaxy Publication

N-Substituted Indole-2-carboxylates Bearing Rhodanine Moiety: Design, Synthesis, and Evaluation as Antimicrobial Agents with In Silico Insights

Lucas Almeida[1]*, Renata Souza[1]

[1]Department of Drug Development, Faculty of Pharmacy, University of São Paulo, São Paulo, Brazil.

***E-mail** ✉ lucas.almeida@outlook.com

Received: 29 May 2025; **Revised:** 26 August 2025; **Accepted:** 01 September 2025

ABSTRACT

Seventeen novel derivatives of (Z)-methyl 3-(4-oxo-2-thioxothiazolidin-5-ylidene)methyl)-1H-indole-2-carboxylate were synthesized and tested for antimicrobial properties. These compounds demonstrated remarkably potent antibacterial activity against eight different bacterial strains, significantly outperforming the standard antibiotics ampicillin and streptomycin by factors of 10 to 50. Compound 8 was identified as the most effective antibacterial agent. Furthermore, the compounds showed good to excellent antifungal activity, with Compound 15 being the most potent against various fungi. Computational docking studies suggest the antibacterial mechanism involves inhibiting the *E. coli* MurB enzyme, and the antifungal action is likely due to the inhibition of the CYP51Ca lanosterol 14α\alphaα-demethylase. Preliminary studies on drug-likeness, ADMET properties, and cytotoxicity against normal human cells (MRC5) were also completed.

Keywords: Rhodanine, Indole, Antibacterial activity, Antimicrobial, Molecular docking, ADMET

How to Cite This Article: Almeida L, Souza R. N-Substituted Indole-2-carboxylates Bearing Rhodanine Moiety: Design, Synthesis, and Evaluation as Antimicrobial Agents with In Silico Insights. Pharm Sci Drug Des. 2025;5:335-59. https://doi.org/10.51847/OVZk4JLf3T

Introduction

Infectious diseases pose a significant and ongoing threat to global public health security and cause widespread socioeconomic disruption worldwide. For centuries, they have been a primary cause of death and disability for millions of people.

While antimicrobial drugs have historically been crucial in treating life-threatening infections, their effectiveness is now being undermined. The rapid rise of multidrug-resistant bacterial pathogens, coupled with the emergence of new infectious diseases, threatens to diminish the utility of existing approved treatments [1, 2]. Concurrently, fungal infections are a major cause of mortality, responsible for approximately 1.5 million global deaths annually [3]. Treating these fungal diseases is difficult because resistance to current antifungal drugs is increasing, particularly in vulnerable groups such as immunosuppressed patients (e.g., those with cancer, undergoing transplants, or living with HIV) and individuals receiving antimitotic treatments. This situation creates an immediate demand for the discovery of new agents effective against invasive microbial infections.

Aromatic heterocyclic structures have proven to be valuable frameworks for synthesizing numerous bioactive compounds exhibiting antibacterial, antifungal, antiviral, and anti-parasitic properties [4]. Within this field, thiazolidine-2,4-diones (often called glitazones) have become the most prominent subgroup of 4-thiazolidinone compounds over the last several decades [5]. Several medications derived from this heterocyclic class, including Lobeglitazone, Pioglitazone, Rosiglitazone, and Epalrestat, are widely used as oral medications for managing type 2 diabetes. More recently, Ponesimod was approved for the treatment of multiple sclerosis and psoriasis **(Figure 1).**

© 2025 Pharmaceutical Sciences and Drug Design

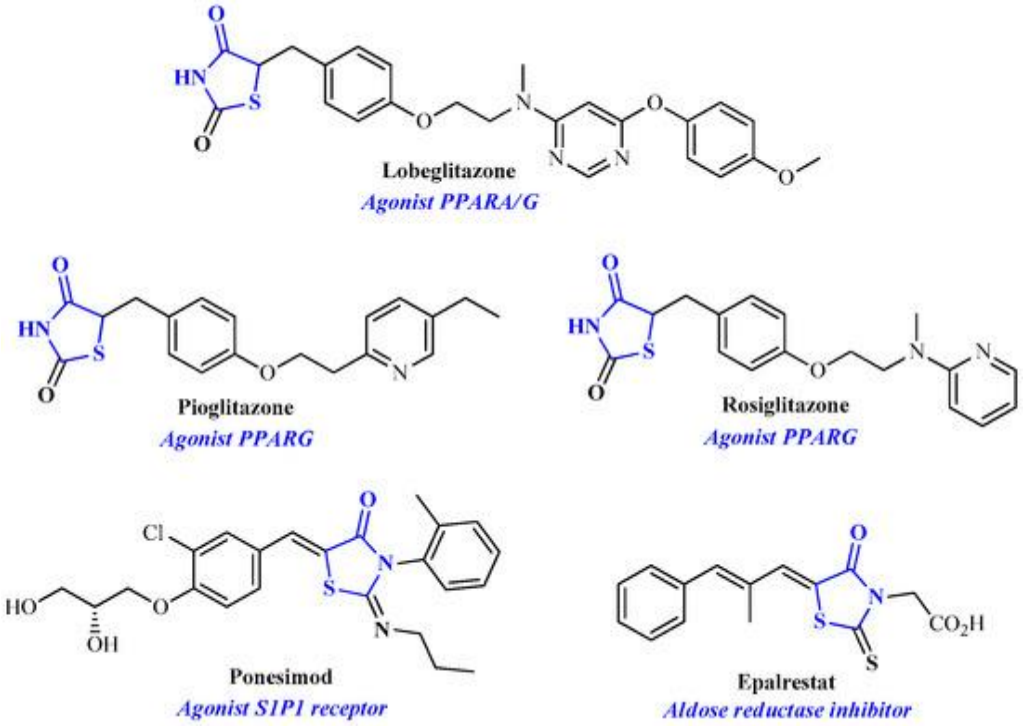

Figure 1. illustrates the chemical structures of several approved drugs that incorporate the 4-thiazolidinone scaffold.

Furthermore, rhodanine derivatives (a subclass of 2-thioxo-4-thiazolidinones) exhibit a wide array of pharmacological effects, including antimicrobial [6-9], anticancer [10-12], anti-HIV [13, 14], antidiabetic [15, 16], antitubercular [17], and immunoproteasome inhibitory [18] activities. This highlights the significant role of this structural motif in medicinal chemistry and drug development.

Another highly promising heterocyclic core is the indole ring, which has garnered substantial interest due to its occurrence in proteins, amino acids, and numerous bioactive natural alkaloids [19]. Indole derivatives display an extensive range of biological properties [20-35], notably including antimicrobial effects [36-41]. Moreover, the indole moiety is a key component in many marketed pharmaceuticals **(Figure 2).**

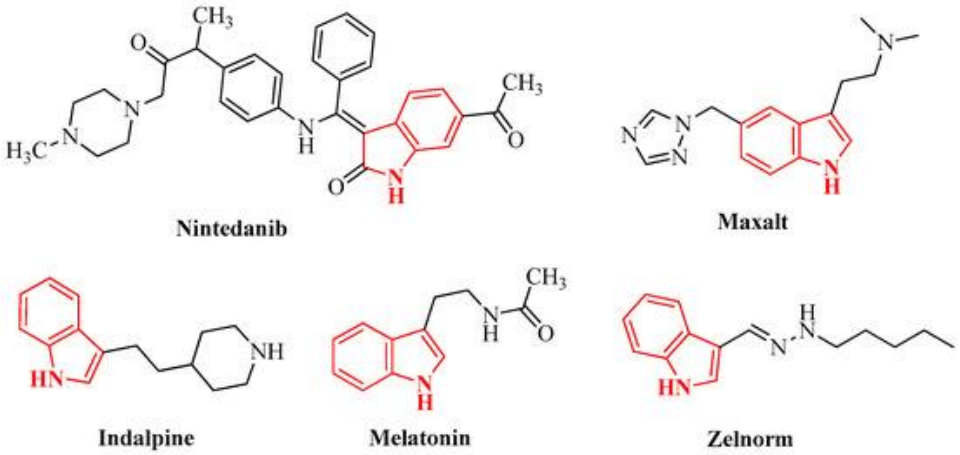

Figure 2. depicts the chemical structures of several approved drugs that feature the indole scaffold.

In recent years, the strategy of developing hybrid molecules—by covalently linking two or more pharmacophoric units within a single molecular architecture—has gained significant momentum. Several studies have highlighted the role of cooperative hydrogen bonding in antibiotics, as well as the molecular hybridization of sugar-conjugated indoles [42, 43].

Given that this hybridization approach can yield compounds capable of targeting multiple biological sites simultaneously, we directed our research toward identifying new antibacterial and antifungal candidates based on this principle [44].

To date, numerous indole-rhodanine hybrids **(Figure 3)** have been reported [6, 41, 45-49] with antimicrobial properties, including some that exhibit potent activity against multidrug-resistant pathogens [6, 41, 47-49]. Thus, integrating the indole and rhodanine moieties into novel chemical entities represents a potentially effective approach for advancing antimicrobial treatments. Building on this concept, in our earlier work [6, 41], we outlined the design and synthesis of prospective antimicrobial compounds incorporating both indole and rhodanine fragments. In the present study, we describe the synthesis, antimicrobial activity assessment, molecular docking investigations, and in silico predictions of pharmacokinetic and toxicity profiles for these compounds.

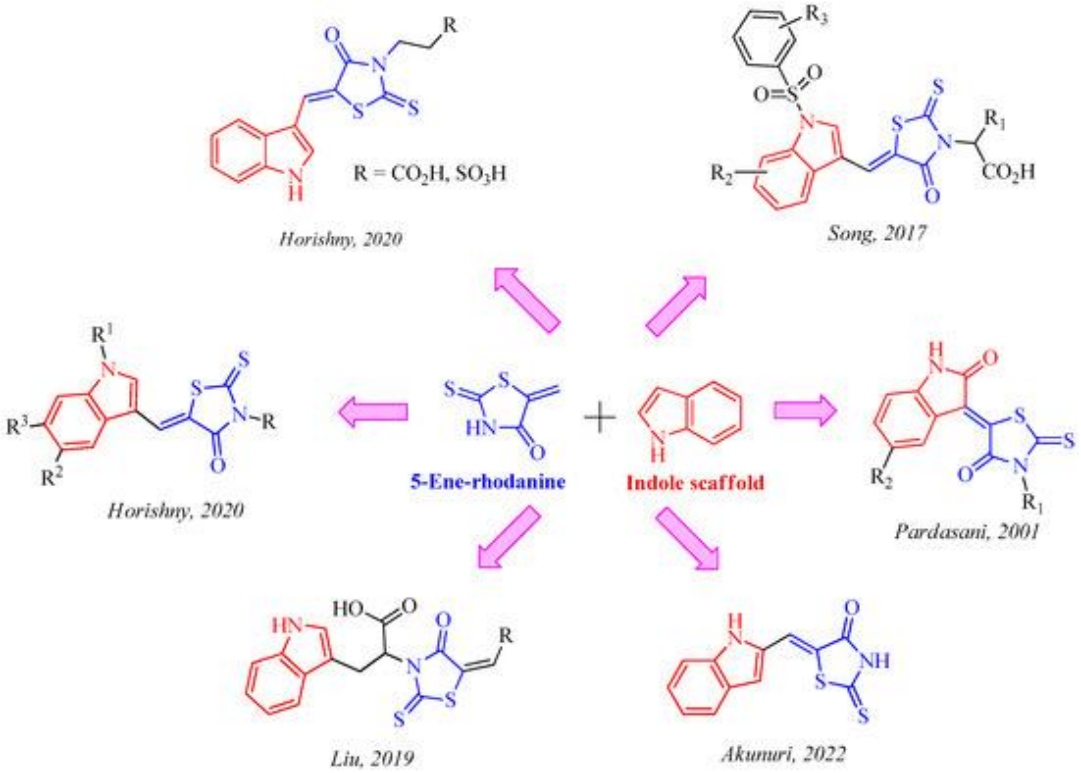

Figure 3. Examples of antimicrobial agents featuring both indole and rhodanine scaffolds [6, 41-49].

Materials and Methods

In silico toxicity assessment

Potential toxicity profiles were evaluated computationally via the ProTox-II online platform [50].

Synthetic procedures and characterization

^{1}H and ^{13}C NMR data were acquired on either a Varian Mercury VX-400 instrument or a Bruker AM-300 (300 MHz) spectrometer, with samples dissolved in DMSO-d_6. Proton chemical shifts were calibrated against the residual DMSO signal at δ 2.50 ppm, and J values are expressed in Hz. Peak assignments relied on two-dimensional NMR methods. Melting point measurements were carried out on an uncorrected Fisher-Johns apparatus (Fisher Scientific, Hampton, NH, USA). Carbon, hydrogen, and nitrogen contents were determined through standard microanalytical procedures.

The target compounds were prepared by adapting a previously published protocol from our group [6].

In the initial step, the selected amino acid (50 mmol) was dissolved in a chilled aqueous KOH solution (20 mL; increased to 150 mmol for di-carboxylic acids), followed by addition of excess carbon disulfide. The mixture was agitated in an open flask until complete homogenization occurred. Next, a neutralized solution of monochloroacetic acid (55 mmol, prepared with 55 mmol sodium bicarbonate in 25 mL water) was introduced gradually while stirring. The reaction was then maintained at ambient temperature for 48 hours.

Acidification was achieved by adding 20 mL of 6N hydrochloric acid, after which the mixture was brought to reflux and gently boiled for 60 minutes. Upon cooling to room temperature, the solid product was isolated by filtration, thoroughly dried, and subjected to multiple recrystallizations using dilute acetic acid, ethanol, and toluene in sequence.

For the condensation step, a round-bottom flask with reflux setup was charged with 2.5 mmol of the appropriate methyl 3-formyl-5,6-disubstituted-1H-indole-2-carboxylate derivative, 3.3 mmol of the corresponding 3-substituted-2-thioxothiazolidin-4-one, 2.5 mmol ammonium acetate, and 5 mL glacial acetic acid. The suspension was heated at reflux for 2 hours. After cooling, the crude product was collected via filtration, rinsed successively with acetic acid and distilled water, dried under vacuum, and further purified by recrystallization.

- (Z)-6-(5-((2-(methoxycarbonyl)-1H-indol-3-yl)methylene)-4-oxo-2-thioxothiazolidin-3-yl)hexanoic acid (**1**). m.p. 135–138 °C. ^{1}H NMR (300 MHz, DMSO-d6) δ 12.06 (s, 2H,NH, OH), 8.49 (s, 1H), 7.79 (s, 1H), 7.58 (s, 1H), 7.35 (s, 1H), 7.24 (s, 1H), 4.09 (s, 2H), 4.00 (s, 3H, CH_3), 2.21 (s, 2H), 1.75 (s, 2H), 1.65 (s, 2H), 1.45 (s, 2H). Anal. Calcd. For $C_{20}H_{20}N_2O_5S_2$ (%): C, 55.54; H, 4.66; N, 6.48; O, 18.50. Found (%): C, 55.50; H, 4.69; N, 6.52; O, 18.47.
- (Z)-4-(5-((2-(methoxycarbonyl)-1H-indol-3-yl)methylene)-4-oxo-2-thioxothiazolidin-3-yl)benzoic acid (**2**). m.p. 294–295 °C. ^{1}H NMR (300 MHz, DMSO-d6) δ 12.69 (s, 1H, OH), 8.51 (s, 1H), 8.16 (d, J = 8.1 Hz, 2H), 7.87 (d, J = 8.2 Hz, 1H), 7.60 (d, J = 8.1 Hz, 1H), 7.47 (d, J = 8.2 Hz, 2H), 7.37 (t, J = 7.6 Hz, 1H), 7.28 (t, J = 7.5 Hz, 1H), 4.00 (s, 3H, CH_3). Anal. Calcd. For $C_{21}H_{14}N_2O_5S_2$ (%): C, 57.52; H, 3.22; N, 6.39; O, 18.24. Found (%): C, 57.54; H, 3.20; N, 6.42; O, 18.25.
- (Z)-methyl 3-((3-(3-hydroxyphenyl)-4-oxo-2-thioxothiazolidin-5-ylidene)methyl)-1H-indole-2-carboxylate (**3**). m.p. 245–247 °C. ^{1}H NMR (300 MHz, DMSO-d6) δ 12.66 (s, 1H, OH), 9.61 (s, 1H, NH), 8.48 (s, 1H), 7.87 (d, J = 8.2 Hz, 1H), 7.59 (d, J = 8.3 Hz, 1H), 7.31 (dq, J = 7.2, 22.3 Hz, 3H), 6.90 (d, J = 8.4 Hz, 1H), 6.71 (d, J = 5.2 Hz, 2H), 4.00 (s, 3H,CH_3). Anal. Calcd. For $C_{20}H_{14}N_2O_4S_2$ (%): C, 58.52; H, 3.44; N, 6.82; O, 15.59. Found (%): C, 58.50; H, 3.43; N, 6.87; O, 15.53.
- (Z)-methyl 3-((3-(4-hydroxyphenyl)-4-oxo-2-thioxothiazolidin-5-ylidene)methyl)-1H-indole-2-carboxylate (**4**). m.p. 282–284 °C. ^{1}H NMR (300 MHz, DMSO-d6) δ 12.64 (s, 1H, OH), 9.62 (s, 1H, NH), 8.47 (s, 1H), 7.86 (d, J = 8.2 Hz, 1H), 7.59 (d, J = 8.3 Hz, 1H), 7.36 (t, J = 7.7 Hz, 1H), 7.26 (t, J = 7.6 Hz, 1H), 7.08 (d, J = 8.3 Hz, 2H), 6.90 (d, J = 8.3 Hz, 2H), 4.00 (s, 3H, CH_3). Anal. Calcd. For $C_{20}H_{14}N_2O_4S_2$ (%): C, 58.52; H, 3.44; N, 6.82; O, 15.59. Found (%): C, 58.50; H, 3.47; N, 6.86; O, 15.55.
- (Z)-methyl 3-((3-(3-morpholinopropyl)-4-oxo-2-thioxothiazolidin-5-ylidene)methyl)-1H-indole-2-carboxylate (**5**). m.p. 213–214 °C. ^{1}H NMR (300 MHz, DMSO-d6) δ 12.64 (s, 1H, NH), 8.47 (s, 1H), 7.78 (d, J = 8.2 Hz, 1H), 7.58 (d, J = 8.3 Hz, 1H), 7.35 (t, J = 7.6 Hz, 1H), 7.24 (t, J = 7.6 Hz, 1H), 4.18 (t, J = 7.0 Hz, 2H), 4.00 (s, 2H), 3.55 (t, J = 4.6 Hz, 4H, CH_3), 2.58–2.29 (m, 8H), 1.89 (p, J = 6.8 Hz, 2H). Anal. Calcd. For $C_{21}H_{23}N_3O_4S_2$ (%): C, 56.61; H, 5.20; N, 9.43; O, 14.36. Found (%): C, 56.64; H, 5.18; N, 9.45; O, 14.30.
- (Z)-methyl 3-((3-morpholino-4-oxo-2-thioxothiazolidin-5-ylidene)methyl)-1H-indole-2-carboxylate (**6**). m.p. 278–280 °C. ^{1}H NMR (300 MHz) δ 12.65 (s, 1H, NH), 8.42 (s, 1H), 7.78 (d, J = 8.1 Hz, 1H), 7.57 (d, J = 8.3 Hz, 1H), 7.34 (t, J = 7.7 Hz, 1H), 7.23 (t, J = 7.6 Hz, 1H), 4.00 (s, 3H, CH_3), 3.05 (d, J = 22.9 Hz, 4H), 2.50 (s, 3H). Anal. Calcd. For $C_{18}H_{17}N_3O_4S_2$ (%): C, 53.58; H, 4.25; N, 10.41; O, 15.86. Found (%): C, 53.60; H, 4.21; N, 10.46; O, 15.83.
- (Z)-methyl 3-((3-(furan-2-ylmethyl)-4-oxo-2-thioxothiazolidin-5-ylidene)methyl)-1H-indole-2-carboxylate (**7**). ^{1}H NMR (300 MHz, DMSO-d6) δ 12.65 (s, 1H, NH), 8.52 (s, 1H), 7.79 (d, J = 8.2 Hz, 1H), 7.57 (d, J = 8.2 Hz, 1H), 7.47 (s, 1H), 7.34 (t, J = 7.7 Hz, 1H), 7.23 (t, J = 7.6 Hz, 1H), 6.41 (s, 1H), 6.36 (s, 1H), 5.26 (s, 2H), 4.00 (s, 3H, CH_3). m.p. 212–213 °C. Anal. Calcd. For $C_{19}H_{14}N_2O_4S_2$ (%): C, 57.27; H, 3.54; N, 7.03; O, 16.06. Found (%): C, 57.31; H, 3.50; N, 7.08; O, 16.02.
- (Z)-2-(5-((5-fluoro-2-(methoxycarbonyl)-1H-indol-3-yl)methylene)-4-oxo-2-thioxothiazolidin-3-yl)-3-methylbutanoic acid (**8**). ^{1}H NMR (300 MHz, DMSO-d6) δ 8.44 (s, 1H, NH), 7.58 (dd, J = 4.7, 9.0 Hz, 1H), 7.48 (d, J = 9.7 Hz, 1H), 7.15 (t, J = 9.2 Hz, 1H), 5.12 (d, J = 9.6 Hz, 1H), 4.00 (s, 3H, O-CH_3), 2.80 (s, 1H, CH-(CH_3)$_2$), 1.28 (d, J = 6.2 Hz, 3H, CH-CH_3), 0.84 (d, J = 6.7 Hz, 3H, CH-CH_3). m.p. 234–235 °C. Anal. Calcd. For $C_{19}H_{17}FN_2O_5S_2$ (%): C, 52.28; H, 3.93; F, 4.35; N, 6.42; O, 18.33. Found (%): C, 52.23; H, 3.90; F, 4.28; N, 6.54; O, 18.29.

- (Z)-4-(5-((5-fluoro-2-(methoxycarbonyl)-1H-indol-3-yl)methylene)-4-oxo-2-thioxothiazolidin-3-yl)butanoic acid (**9**). m.p. 192–193 °C. ^{1}H NMR (300 MHz, DMSO-d6) δ 12.72 (s, 1H, NH), 11.90 (s, 1H, OH), 8.38 (s, 1H), 7.57 (dd, J = 4.7, 9.0 Hz, 1H), 7.46 (dd, J = 2.3, 9.9 Hz, 1H), 7.14 (td, J = 2.5, 9.1 Hz, 1H), 4.14 (t, J = 7.0 Hz, 2H), 3.99 (s, 3H, CH_3), 2.32 (t, J = 7.4 Hz, 2H), 1.98 (p, J = 7.4 Hz, 2H). Anal. Calcd. For $C_{18}H_{15}FN_2O_5S_2$ (%): C, 51.18; H, 3.58; F, 4.50; N, 6.63; O, 18.94. Found (%): C, 51.23; H, 3.55; F, 4.48; N, 6.69; O, 18.90.
- (Z)-methyl 5-fluoro-3-((3-(4-hydroxyphenyl)-4-oxo-2-thioxothiazolidin-5-ylidene)methyl)-1H-indole-2-carboxylate (**10**). m.p. 267–268 °C. ^{1}H NMR (300 MHz, DMSO-d6) δ 12.74 (s, 1H, OH), 9.61 (s, 1H, NH), 8.37 (s, 1H), 7.64 – 7.47 (m, 2H), 7.15 (t, J = 8.7 Hz, 1H), 7.07 (d, J = 8.4 Hz, 2H), 6.90 (d, J = 8.4 Hz, 2H), 3.99 (s, 3H, O-CH_3). Anal. Calcd. For $C_{20}H_{13}FN_2O_4S_2$ (%): C, 56.06; H, 3.06; F, 4.43; N, 6.54; O, 14.94. Found (%): C, 56.12; H, 3.02; F, 4.39; N, 6.58; O, 14.87.
- (Z)-2-(5-((2-(methoxycarbonyl)-1H-indol-3-yl)methylene)-4-oxo-2-thioxothiazolidin-3-yl)acetic acid (**11**). m.p. 292–294 °C. ^{1}H NMR (300 MHz, DMSO-d6) δ 8.51 (s, 1H), 7.80 (d, J = 8.3 Hz, 1H), 7.57 (d, J = 8.3 Hz, 1H), 7.34 (t, J = 7.6 Hz, 1H), 7.24 (t, J = 7.6 Hz, 1H), 4.65 (s, 2H), 3.99 (s, 3H,O-CH_3). Anal. Calcd. For $C_{16}H_{12}N_2O_5S_2$ (%): C, 51.05; H, 3.21; N, 7.44; O, 21.25. Found (%): C, 51.11; H, 3.27; N, 7.33; O, 21.20.
- (Z)-2-(5-((2-(methoxycarbonyl)-1H-indol-3-yl)methylene)-4-oxo-2-thioxothiazolidin-3-yl)-3-methylbutanoic acid (**12**). m.p. 256–258 °C. ^{1}H NMR (300 MHz, DMSO-d6) δ 8.51 (s, 1H), 7.82 (d, J = 8.2 Hz, 1H), 7.58 (d, J = 8.2 Hz, 1H), 7.34 (t, J = 7.7 Hz, 1H), 7.24 (t, J = 7.6 Hz, 1H), 5.13 (d, J = 9.2 Hz, 1H), 4.00 (s, 3H), 2.79 (s, 1H, CH-(CH_3)$_2$), 1.28 (d, J = 6.3 Hz, 3H, CH-CH_3), 0.84 (d, J = 6.8 Hz, 3H, CH-CH_3). Anal. Calcd. For $C_{19}H_{18}N_2O_5S_2$ (%): C, 54.53; H, 4.34; N, 6.69; O, 19.12. Found (%): C, 54.49; H, 4.37; N, 6.71; O, 19.10.
- (Z)-methyl 3-((3-(3-fluorophenyl)-4-oxo-2-thioxothiazolidin-5-ylidene)methyl)-6-methoxy-1H-indole-2-carboxylate (**13**). m.p. 238–240 °C. ^{1}H NMR (300 MHz, DMSO-d6) δ 12.65 (s, 1H, NH), 8.52 (s, 1H), 7.79 (d, J = 8.2 Hz, 1H), 7.57 (d, J = 8.2 Hz, 1H), 7.47 (s, 1H), 7.34 (t, J = 7.7 Hz, 1H), 7.23 (t, J = 7.6 Hz, 1H), 6.41 (s, 1H), 6.36 (s, 1H), 5.26(s, 3H, O-CH_3), 4.00 (s, 3H, O-CH_3). Anal. Calcd. For $C_{21}H_{15}FN_2O_4S_2$ (%): C, 57.00; H, 3.42; F, 4.29; N, 6.33; O, 14.46. Found (%): C, 57.12; H, 3.39; F, 4.32; N, 6.38; O, 14.51.
- (Z)-3-(5-((5-fluoro-2-(methoxycarbonyl)-1H-indol-3-yl)methylene)-4-oxo-2-thioxothiazolidin-3-yl)propanoic acid (**14**). m.p. 275–276 °C. ^{1}H NMR (300 MHz, DMSO-d6) δ 12.76 (s, 1H, OH), 12.30 (s, 1H, NH), 8.39 (s, 1H), 7.57 (dd, J = 4.6, 9.0 Hz, 1H), 7.44 (d, J = 9.8 Hz, 1H), 7.15 (t, J = 8.9 Hz, 1H), 4.29 (t, J = 7.9 Hz, 2H), 3.99 (s, 3H, CH_3), 2.64 (t, J = 8.1 Hz, 2H). Anal. Calcd. For $C_{17}H_{13}FN_2O_5S_2$ (%): C, 49.99; H, 3.21; F, 4.65; N, 6.86; O, 19.59. Found (%): C, 49.92; H, 3.25; F, 4.60; N, 6.90; O, 19.62.
- (Z)-methyl 5-fluoro-3-((3-methyl-4-oxo-2-thioxothiazolidin-5-ylidene)methyl)-1H-indole-2-carboxylate (**15).** m.p. 234–244 °C. ^{1}H NMR (300 MHz) δ 12.75 (s, 1H, NH), 8.40 (s, 1H), 7.57 (dd, J = 4.7, 9.0 Hz, 1H), 7.43 (d, J = 9.7 Hz, 1H), 7.15 (t, J = 9.0 Hz, 1H), 3.99 (s, 3H, O-CH_3), 3.48 (s, 3H, N-CH_3). Anal. Calcd. For $C_{15}H_{11}FN_2O_3S_2$ (%): C, 51.42; H, 3.16; F, 5.42; N, 7.99; O, 13.70. Found (%): C, 51.40; H, 3.21; F, 5.45; N, 7.93; O, 13.75.
- (Z)-methyl 5-fluoro-3-((3-morpholino-4-oxo-2-thioxothiazolidin-5-ylidene)methyl)-1H-indole-2-carboxylate (**16**). m.p. 273–274 °C. ^{1}H NMR (300 MHz, DMSO-d6) δ 12.76 (s, 1H, NH), 8.32 (s, 1H), 7.57 (dd, J = 4.6, 9.1 Hz, 1H), 7.46 (d, J = 9.6 Hz, 1H), 7.15 (t, J = 9.1 Hz, 1H), 4.00 (s, 3H, CH_3), 3.77 (dd, J = 16.8, 29.8 Hz, 6H), 3.05 (d, J = 26.1 Hz, 3H). Anal. Calcd. For $C_{18}H_{16}FN_3O_4S_2$ (%): C, 51.30; H, 3.83; F, 4.51; N, 9.97; O, 15.18. Found (%): C, 51.36; H, 3.79; F, 4.54; N, 9.93; O, 15.21.
- (Z)-3-(5-((2-(methoxycarbonyl)-1H-indol-3-yl)methylene)-4-oxo-2-thioxothiazolidin-3-yl)propanoic acid (**17**). m.p. 265–266 °C. ^{1}H NMR (300 MHz, DMSO-d6) δ 12.65 (s, 1H, NH), 12.30 (s, 1H, OH), 8.49 (s, 1H), 7.78 (d, J = 8.2 Hz, 1H), 7.57 (d, J = 8.3 Hz, 1H), 7.35 (t, J = 7.7 Hz, 1H), 7.24 (t, J = 7.4 Hz, 1H), 4.29 (t, J = 7.9 Hz, 2H), 4.00 (s, 3H, O-CH_3), 2.64 (t, J = 8.1 Hz, 2H). Anal. Calcd. For $C_{17}H_{14}N_2O_5S_2$ (%): C, 52.30; H, 3.61; N, 7.17; O, 20.49. Found (%): C, 52.28; H, 3.65; N, 7.21; O, 20.52.

Bioactivity testing

Evaluation of antibacterial effects

The study included several bacterial strains: Gram-negative ones such as Escherichia coli (ATCC 35210), Enterobacter cloacae (clinical isolate), and Salmonella typhimurium (ATCC 13311); and Gram-positive ones including Listeria monocytogenes (NCTC 7973), Bacillus cereus (clinical isolate), and Staphylococcus aureus

(ATCC 6538). All strains were supplied by the Mycological Laboratory at the Department of Plant Physiology, Institute for Biological Research "Siniša Stanković" in Belgrade, Serbia. Determination of the lowest concentrations that inhibit growth (MIC) and kill bacteria (MBC) was done via an adapted microdilution approach, following methods outlined previously [6, 41].

Evaluation of antifungal effects

Antifungal screening was conducted against six species: Aspergillus niger (ATCC 6275), Aspergillus fumigatus (ATCC 1022), Aspergillus versicolor (ATCC 11730), Penicillium funiculosum (ATCC 36839), Trichoderma viride (IAM 5061), and Penicillium verrucosum var. cyclopium (food isolate). These were also provided by the Mycological Laboratory, Department of Plant Physiology, Institute for Biological Research "Siniša Stanković", Belgrade, Serbia. Experiments were repeated twice for reliability [51, 52].

Molecular docking simulations

Computational docking was carried out with AutoDock 4.2®; the full protocol is described in our earlier work [53].

Prediction of drug-like properties

To evaluate potential as drug candidates, five predictive models were applied [54] using Molsoft tools and the SwissADME web tool (<http://swissadme.ch>, accessed on 25 October 2022), with molecular structures drawn via ChemAxon's Marvin JS interface.

ADMET Profiling

In silico forecasts of absorption, distribution, metabolism, excretion, and toxicity (covering aspects like phospholipidosis and hERG-related cardiotoxicity) were generated with ADMET Predictor version 10.4 [54-57].

Cytotoxicity testing

MRC-5 human fetal lung fibroblasts (passages below 40) were cultured in the Laboratory of Pharmacology (Dr. I.S. Vizirianakis), School of Pharmacy, Aristotle University of Thessaloniki, Greece, according to established procedures [58]. The cells were kept at 37 °C in a 5% CO_2 humidified incubator using DMEM medium supplemented with 10% fetal bovine serum and 1% penicillin-streptomycin. Compounds were dissolved in DMSO and refrigerated at 4 °C. For testing, cells were plated in 96-well formats at a density of 5×10^4 cells/mL, incubated for 20 hours to adhere, then treated with compounds at 0.1 μM, 1 μM, or 10 μM. DMSO levels remained at 0.02% v/v, showing no influence on viability. After 48 hours of exposure, viability was measured by adding CCK-8 reagent (Sigma-Aldrich, St. Louis, MO, USA) and incubating for another 4 hours at 37 °C before reading absorbance at 450 nm on a plate reader. Blanks included only the reagent. Values represent averages ± SD from three replicates. Data analysis involved t-tests and ANOVA in SPSS software, considering differences significant at $p < 0.05$.

Results and Discussion

In silico toxicity assessment

Evaluating potential toxicity early is essential in drug development. Computational (in silico) methods provide a rapid and efficient alternative to animal testing, while also minimizing the need for subsequent in vivo studies. Here, we conducted in silico toxicity screening for compounds 1–17 prior to experimental testing, allowing us to flag and eliminate any candidates with unfavorable safety profiles.

Toxicity predictions were generated using the ProTox-II online platform, which assessed multiple endpoints including acute toxicity in rats, hepatotoxicity, cytotoxicity, carcinogenicity, mutagenicity, immunotoxicity, and Tox21 pathway disruptions. Complementary analysis with ADMET Predictor 10.4 (Simulation Plus) addressed additional risks, notably phospholipidosis and hERG-mediated cardiotoxicity.

Oral acute toxicity is typically reported as the LD50 value (mg/kg body weight), representing the dose lethal to 50% of exposed animals. The Globally Harmonized System (GHS) categorizes chemicals into toxicity classes: Class I: fatal if swallowed ($LD50 \leq 5$ mg/kg); Class II: fatal if swallowed (5 mg/kg $< LD50 \leq 50$ mg/kg); Class III: toxic if swallowed (50 mg/kg $< LD50 \leq 300$ mg/kg); Class IV: harmful if swallowed (300 mg/kg $< LD50 \leq$

2000 mg/kg); Class V: may be harmful if swallowed (2000 mg/kg < LD50 ≤ 5000 mg/kg); Class VI: non-toxic (LD50 > 5000 mg/kg).

Our computational results (prediction confidence 54–66%) placed all compounds in Class IV, indicating an acceptable acute oral toxicity profile in rats. No compound was flagged for adverse effects across the evaluated Tox21 pathways.

Synthesis

All target compounds were obtained using the synthetic route previously reported by our group [41] and summarized in **Scheme 1**. Their structures are shown in **Table 1**. Structural confirmation was achieved via ^{1}H and ^{13}C NMR spectroscopy together with elemental analysis; full spectroscopic and analytical data are included in the Experimental Section.

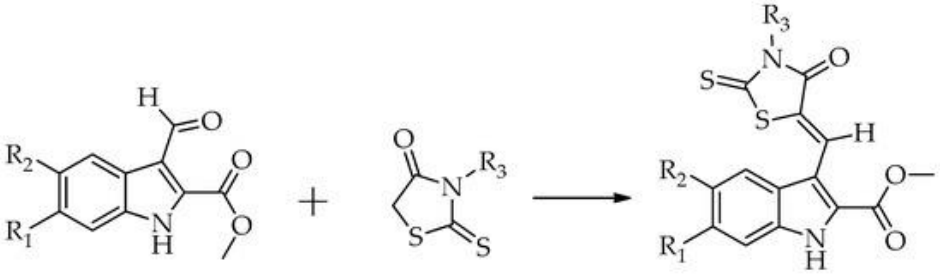

Scheme 1. Synthesis of target compounds 1–17. Conditions and Reagents: CH_3COOH, CH_3COONH_4, reflux 2 h.

Table 1. Chemical structures of the compounds subjected to biological evaluation.

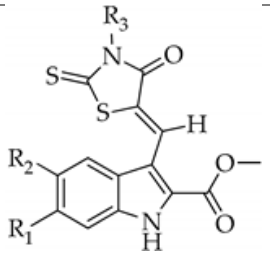

Compound	R^1	R^2	R^3
1	H	H	$-(CH_2)_5CO_2H$
2	H	H	4-carboxyphenyl
3	H	H	3-hydroxyphenyl
4	H	H	4-hydroxyphenyl
5	H	H	4-propylmorpholin-4-yl
6	H	H	morpholin-4-yl
7	H	H	(2-methylfuran-3-yl)
8	H	F	$-C(CH_3)_2CO_2H$
9	H	F	$-(CH_2)_3CO_2H$
10	H	F	4-hydroxyphenyl
11	H	H	$-CH_2CO_2H$
12	H	H	$-C(CH_3)_2CO_2H$
13	$-OCH_3$	H	3-fluorophenyl
14	H	F	$-(CH_2)_2CO_2H$
15	H	F	$-CH_3$
16	H	F	morpholin-4-yl
17	H	H	$-(CH_2)_2CO_2H$

Biological evaluation

Antimicrobial activity

All synthesized compounds listed in **Table 1** were tested for their ability to inhibit the growth of eight bacterial strains employing the broth microdilution assay. Ampicillin and streptomycin were included as positive controls. The series exhibited strong to outstanding antibacterial effects, achieving minimum inhibitory concentrations (MICs) between 0.004 and 0.045 mg/mL and minimum bactericidal concentrations (MBCs) between 0.008 and 1.2 mg/mL **(Table 2).** Ranking the compounds by overall potency yielded the following sequence: 8 > 11 > 2 > 1 > 12 > 3 > 17 > 7 > 5 > 13 > 14 > 16 > 9 > 4 = 6 > 15 > 10. The lead compound, 8, stood out with MICs of 0.004–0.03 mg/mL and MBCs of 0.008–0.06 mg/mL across the panel, while compound 10 showed the lowest potency. Several derivatives displayed notable strain-specific activity. For instance, compounds 1, 2, and 3 effectively inhibited Bacillus cereus at an MIC of 0.015 mg/mL. Compounds 2–7 were particularly active against Staphylococcus aureus, compounds 8 and 12 against Listeria monocytogenes, and compounds 2–6 plus 12 against Enterobacter cloacae. Against Salmonella typhimurium, compounds 1, 3, 7, 11, and 12 achieved an MIC of 0.015 mg/mL. Compounds 1 and 11 performed well against Escherichia coli, while compounds 8 and 12 reached exceptionally low MICs of 0.004 mg/mL against Enterobacter cloacae and Escherichia coli, respectively. Compounds 11 and 17 inhibited Bacillus cereus and Staphylococcus aureus at 0.008 mg/mL, and compound 11 also targeted Enterobacter cloacae and Pseudomonas aeruginosa effectively (MIC 0.011 mg/mL). Crucially, every compound in the series surpassed the activity of both reference antibiotics against all tested strains. Enterobacter cloacae emerged as the most vulnerable bacterium, whereas Escherichia coli displayed the greatest resistance, closely followed by Micrococcus flavus.

Table 2. Antibacterial potency of the synthesized compounds (MIC and MBC values in mg/mL).

Compound		Bacillus cereus	Staphylococcus aureus	Listeria monocytogenes	Micrococcus flavus	Escherichia coli	Pseudomonas aeruginosa	Salmonella typhimurium	Enterobacter cloacae
1	MIC	0.015 ± 0.009	0.022 ± 0.005	0.022 ± 0.004	0.022 ± 0.005	0.015 ± 0.009	0.022 ± 0.005	0.015 ± 0.009	0.022 ± 0.005
	MBC	0.03 ± 0.01	0.03 ± 0.01	0.06 ± 0.006	0.03 ± 0.01	0.03 ± 0.01	0.06 ± 0.006	0.03 ± 0.01	0.03 ± 0.01
2	MIC	0.015 ± 0.009	0.015 ± 0.009	0.03 ± 0.01	0.022 ± 0.005	0.022 ± 0.005	0.03 ± 0.01	0.022 ± 0.005	0.015 ± 0.009
	MBC	0.03 ± 0.01	0.03 ± 0.01	0.06 ± 0.006	0.03 ± 0.01	0.03 ± 0.01	0.06 ± 0.006	0.03 ± 0.01	0.03 ± 0.01
3	MIC	0.015 ± 0.009	0.015 ± 0.009	0.03 ± 0.01	0.045 ± 0.003	0.022 ± 0.005	0.03 ± 0.01	0.015 ± 0.009	0.015 ± 0.009
	MBC	0.03 ± 0.01	0.03 ± 0.01	0.06 ± 0.006	0.06 ± 0.006	0.03 ± 0.01	0.06 ± 0.006	0.03 ± 0.01	0.03 ± 0.01
4	MIC	0.03 ± 0.01	0.03 ± 0.01	0.045 ± 0.001	0.045 ± 0.003	0.045 ± 0.003	0.03 ± 0.01	0.045 ± 0.003	0.015 ± 0.009
	MBC	0.06 ± 0.006	0.06 ± 0.006	0.06 ± 0.006	0.06 ± 0.006	0.06 ± 0.006	0.06 ± 0.006	0.06 ± 0.006	0.03 ± 0.01
5	MIC	0.03 ± 0.01	0.015 ± 0.009	0.03 ± 0.01	0.045 ± 0.003	0.03 ± 0.01	0.03 ± 0.01	0.022 ± 0.005	0.015 ± 0.009
	MBC	0.06 ± 0.006	0.03 ± 0.01	0.06 ± 0.006	0.06 ± 0.006	0.06 ± 0.006	0.06 ± 0.006	0.03 ± 0.01	0.03 ± 0.01
6	MIC	0.03 ± 0.01	0.015 ± 0.009	0.03 ± 0.01	0.045 ± 0.003	0.06 ± 0.006	0.03 ± 0.01	0.03 ± 0.01	0.015 ± 0.009
	MBC	0.06 ± 0.006	0.03 ± 0.01	0.06 ± 0.006	0.06 ± 0.006	0.12 ± 0.01	0.06 ± 0.006	0.06 ± 0.006	0.03 ± 0.01
7	MIC	0.03 ± 0.01	0.015 ± 0.009	0.03 ± 0.01	0.045 ± 0.003	0.03 ± 0.01	0.03 ± 0.01	0.015 ± 0.009	0.015 ± 0.009
	MBC	0.06 ± 0.006	0.03 ± 0.01	0.06 ± 0.006	0.06 ± 0.006	0.06 ± 0.006	0.06 ± 0.006	0.03 ± 0.01	0.03 ± 0.01

8	MIC	0.03 ± 0.01	0.03 ± 0.01	0.015 ± 0.001	0.03 ± 0.01	0.008 ± 0.001	0.004 ± 0.005	0.008 ± 0.009	0.004 ± 0.005
	MBC	0.06 ± 0.006	0.06 ± 0.006	0.03 ± 0.01	0.06 ± 0.006	0.015 ± 0.009	0.008 ± 0.0006	0.015 ± 0.009	0.008 ± 0.0006
9	MIC	0.03 ± 0.01	0.03 ± 0.01	0.03 ± 0.01	0.03 ± 0.01	0.03 ± 0.01	0.03 ± 0.01	0.03 ± 0.01	0.03 ± 0.01
	MBC	0.06 ± 0.006	0.06 ± 0.006	0.06 ± 0.006	0.06 ± 0.006	0.06 ± 0.006	0.06 ± 0.006	0.06 ± 0.006	0.06 ± 0.006
10	MIC	0.03 ± 0.01	0.03 ± 0.01	0.03 ± 0.01	0.045 ± 0.003	0.03 ± 0.01	0.03 ± 0.01	0.045 ± 0.003	0.03 ± 0.01
	MBC	0.06 ± 0.006	0.06 ± 0.006	0.06 ± 0.006	0.06 ± 0.006	0.06 ± 0.006	0.06 ± 0.006	0.06 ± 0.006	0.06 ± 0.006
11	MIC	0.008 ± 0.0006	0.008 ± 0.0006	0.03 ± 0.01	0.03 ± 0.01	0.015 ± 0.009	0.011 ± 0.01	0.015 ± 0.009	0.011 ± 0.01
	MBC	0.015 ± 0.009	0.015 ± 0.009	0.06 ± 0.006	0.06 ± 0.006	0.03 ± 0.01	0.03 ± 0.01	0.03 ± 0.01	0.03 ± 0.01
12	MIC	0.03 ± 0.01	0.03 ± 0.01	0.015 ± 0.001	0.03 ± 0.01	0.015 ± 0.009	0.015 ± 0.009	0.004 ± 0.005	0.03 ± 0.01
	MBC	0.06 ± 0.006	0.06 ± 0.006	0.03 ± 0.01	0.06 ± 0.006	0.03 ± 0.01	0.03 ± 0.01	0.008 ± 0.009	0.06 ± 0.006
13	MIC	0.03 ± 0.01	0.015 ± 0.009	0.03 ± 0.01	0.045 ± 0.003	0.045 ± 0.003	0.03 ± 0.01	0.03 ± 0.01	0.015 ± 0.009
	MBC	0.06 ± 0.006	0.03 ± 0.01	0.06 ± 0.006	0.06 ± 0.006	0.06 ± 0.006	0.06 ± 0.006	0.06 ± 0.006	0.03 ± 0.01
14	MIC	0.03 ± 0.01	0.03 ± 0.01	0.045 ± 0.003	0.045 ± 0.003	0.045 ± 0.003	0.015 ± 0.009	0.045 ± 0.003	0.015 ± 0.009
	MBC	0.06 ± 0.006	0.06 ± 0.006	0.06 ± 0.006	0.06 ± 0.006	0.06 ± 0.006	0.03 ± 0.01	0.06 ± 0.006	0.03 ± 0.01
15	MIC	0.03 ± 0.01	0.022 ± 0.005	0.045 ± 0.003	0.045 ± 0.003	0.045 ± 0.003	0.03 ± 0.01	0.045 ± 0.003	0.03 ± 0.01
	MBC	0.06 ± 0.006	0.03 ± 0.01	0.06 ± 0.006	0.06 ± 0.006	0.06 ± 0.006	0.06 ± 0.006	0.06 ± 0.006	0.06 ± 0.006
16	MIC	0.015 ± 0.009	0.022 ± 0.005	0.045 ± 0.003	0.045 ± 0.003	0.03 ± 0.01	0.03 ± 0.01	0.045 ± 0.003	0.045 ± 0.003
	MBC	0.03 ± 0.01	0.03 ± 0.01	0.06 ± 0.006	0.06 ± 0.006	0.06 ± 0.006	0.06 ± 0.006	0.06 ± 0.006	0.06 ± 0.006
17	MIC	0.03 ± 0.01	0.008 ± 0.0006	0.03 ± 0.01	0.03 ± 0.01	0.045 ± 0.003	0.008 ± 0.000	0.03 ± 0.01	0.008 ± 0.0006
	MBC	0.06 ± 0.006	0.015 ± 0.00	0.06 ± 0.006	0.06 ± 0.006	0.06 ± 0.006	0.015 ± 0.009	0.06 ± 0.006	0.015 ± 0.009
Streptomycin	MIC	0.0015 ± 0.0002	0.10 ± 0.00	0.15 ± 0.03	0.20 ± 0.00	0.10 ± 0.05	0.10 ± 0.05	0.10 ± 0.05	0.20 ± 0.005
	MBC	0.003 ± 0.0005	0.20 ± 0.00	0.30 ± 0.03	0.30 ± 0.03	0.20 ± 0.00	0.20 ± 0.00	0.20 ± 0.009	0.30 ± 0.03
Ampicillin	MIC	0.006 ± 0.003	0.10 ± 0.05	0.15 ± 0.03	0.25 ± 0.09	0.10 ± 0.05	0.30 ± 0.03	0.15 ± 0.03	0.25 ± 0.09
	MBC	0.025 ± 0.00	0.15 ± 0.05	0.30 ± 0.03	0.50 ± 0.1	0.20 ± 0.00	0.50 ± 0.1	0.20 ± 0.009	0.50 ± 0.1

M.f.—M. flavus, S.t.—S. typhimurium, B.c.—B. cereus, L.m.—L. monocytogenes, S.a.—S. aurues, P.a.—P. aeruginosa, En.c.—En. Cloacae.

The structure–activity relationship (SAR) studies revealed that incorporating 3-methylbutanoic acid as a substituent on the nitrogen of the 2-thioxothiazolidin-4-one ring in compound (Z)-2-(5-((5-fluoro-2-(methoxycarbonyl)-1H-indol-3-yl)methylene)-4-oxo-2-thioxothiazolidin-3-yl)-3-methylbutanoic acid, along with a methylformate group on the indole ring (compound 8), enhances antibacterial properties. Substituting 3-methylbutanoic acid with acetic acid on the nitrogen of the 2-thioxothiazolidin-4-one ring and removing the fluorine atom at position 5 of the indole ring (compound 11) slightly reduced activity. Additionally, replacing the

fluorine with a benzoic acid group at position 5 (compound 2) further decreased antibacterial effectiveness. When the fluorine atom at position 5 was removed from compound 8, resulting in compound 12, its activity decreased, ranking it fifth in terms of antibacterial potency. Furthermore, the presence of a 4-hydroxybenzene substituent on the nitrogen of the 2-thioxothiazolidin-4-one ring negatively affected the compound's antibacterial activity. Overall, these SAR findings demonstrate that the antibacterial activity of these compounds is influenced by the nature of substituents on both the 2-thioxothiazolidin-4-one ring and the indole ring.

Antifungal activity

The antifungal activity of the compounds was tested against eight different fungal species, with ketoconazole and bifonazole serving as reference drugs. The compounds exhibited a range of antifungal activity from good to excellent, with MIC values between 0.004 and 0.06 mg/mL and MFC values between 0.008 and 0.12 mg/mL, as shown in **Table 3.**

Table 3. Antifungal potency of the synthesized compounds (minimum inhibitory concentration (MIC) and minimum fungicidal concentration (MFC) values expressed in mg/mL).

Compound		Aspergillus ochraceus	Aspergillus fumigatus	Aspergillus niger	Aspergillus versicolor	Penicillium ochrochloron	Trichoderma viride	Penicillium verrucosum var. cyclopium
1	MIC	0.008 ± 0.0006	0.06 ± 0.006	0.022 ± 0.005	0.03 ± 0.01	0.004 ± 0.001	0.015 ± 0.003	0.03 ± 0.01
	MFC	0.015 ± 0.003	0.12 ± 0.04	0.03 ± 0.01	0.06 ± 0.006	0.008 ± 0.0006	0.03 ± 0.01	0.06 ± 0.006
2	MIC	0.11 ± 0.01	0.03 ± 0.01	0.022 ± 0.005	0.015 ± 0.003	0.015 ± 0.003	0.008 ± 0.0006	0.03 ± 0.01
	MFC	0.015 ± 0.003	0.06 ± 0.006	0.03 ± 0.01	0.03 ± 0.01	0.03 ± 0.01	0.015 ± 0.003	0.06 ± 0.006
3	MIC	0.008 ± 0.0006	0.03 ± 0.01	0.11 ± 0.01	0.008 ± 0.0006	0.008 ± 0.0006	0.004 ± 0.001	0.015 ± 0.003
	MFC	0.015 ± 0.003	0.06 ± 0.006	0.015 ± 0.003	0.015 ± 0.003	0.015 ± 0.003	0.008 ± 0.0006	0.03 ± 0.01
4	MIC	0.008 ± 0.0006	0.06 ± 0.006	0.015 ± 0.003	0.008 ± 0.0006	0.015 ± 0.003	0.008 ± 0.0006	0.03 ± 0.01
	MFC	0.015 ± 0.003	0.12 ± 0.04	0.03 ± 0.01	0.015 ± 0.003	0.03 ± 0.01	0.015 ± 0.003	0.06 ± 0.006
5	MIC	0.008 ± 0.0006	0.06 ± 0.006	0.015 ± 0.003	0.008 ± 0.0006	0.11 ± 0.01	0.004 ± 0.001	0.015 ± 0.003
	MFC	0.015 ± 0.003	0.12 ± 0.04	0.03 ± 0.01	0.015 ± 0.003	0.015 ± 0.003	0.008 ± 0.0006	0.03 ± 0.01
6	MIC	0.008 ± 0.0006	0.06 ± 0.006	0.11 ± 0.01	0.008 ± 0.0006	0.008 ± 0.0006	0.008 ± 0.0006	0.015 ± 0.003
	MFC	0.015 ± 0.003	0.12 ± 0.04	0.03 ± 0.01	0.015 ± 0.003	0.015 ± 0.003	0.015 ± 0.003	0.03 ± 0.01
7	MIC	0.008 ± 0.0006	0.06 ± 0.006	0.008 ± 0.0006	0.008 ± 0.0006	0.008 ± 0.0006	0.004 ± 0.001	0.015 ± 0.003

	MFC	0.015 ± 0.003	0.12 ± 0.04	0.015 ± 0.003	0.015 ± 0.003	0.015 ± 0.003	0.008 ± 0.0006	0.03 ± 0.01
8	MIC	0.008 ± 0.0006	0.06 ± 0.006	0.015 ± 0.003	0.015 ± 0.003	0.015 ± 0.003	0.11 ± 0.01	0.06 ± 0.006
	MFC	0.015 ± 0.003	0.12 ± 0.04	0.03 ± 0.01	0.03 ± 0.01	0.03 ± 0.01	0.015 ± 0.003	0.12 ± 0.04
9	MIC	0.004 ± 0.001	0.09 ± 0.003	0.015 ± 0.003	0.015 ± 0.003	0.015 ± 0.003	0.008 ± 0.0006	0.022 ± 0.005
	MFC	0.008 ± 0.0006	0.12 ± 0.04	0.03 ± 0.01	0.03 ± 0.01	0.03 ± 0.01	0.015 ± 0.003	0.015 ± 0.003
10	MIC	0.004 ± 0.001	0.06 ± 0.006	0.008 ± 0.0006	0.008 ± 0.0006	0.008 ± 0.0006	0.004 ± 0.001	0.015 ± 0.003
	MFC	0.008 ± 0.0006	0.12 ± 0.04	0.015 ± 0.003	0.015 ± 0.003	0.015 ± 0.003	0.008 ± 0.0006	0.03 ± 0.01
11	MIC	0.008 ± 0.0006	0.06 ± 0.006	0.015 ± 0.003	0.015 ± 0.003	0.015 ± 0.003	0.008 ± 0.0006	0.015 ± 0.003
	MFC	0.015 ± 0.003	0.12 ± 0.04	0.03 ± 0.01	0.03 ± 0.01	0.03 ± 0.01	0.015 ± 0.003	0.03 ± 0.01
12	MIC	0.008 ± 0.0006	0.06 ± 0.006	0.022 ± 0.005	0.008 ± 0.0006	0.015 ± 0.003	0.008 ± 0.0006	0.03 ± 0.01
	MFC	0.015 ± 0.003	0.12 ± 0.04	0.03 ± 0.01	0.015 ± 0.003	0.03 ± 0.01	0.015 ± 0.003	0.06 ± 0.006
13	MIC	0.008 ± 0.0006	0.06 ± 0.006	0.015 ± 0.003	0.015 ± 0.003	0.015 ± 0.003	0.11 ± 0.01	0.015 ± 0.003
	MFC	0.015 ± 0.003	0.12 ± 0.04	0.03 ± 0.01	0.03 ± 0.01	0.03 ± 0.01	0.03 ± 0.01	0.03 ± 0.01
14	MIC	0.015 ± 0.003	0.06 ± 0.006	0.015 ± 0.003	0.015 ± 0.003	0.015 ± 0.003	0.11 ± 0.01	0.015 ± 0.003
	MFC	0.03 ± 0.01	0.12 ± 0.04	0.03 ± 0.01	0.03 ± 0.01	0.03 ± 0.01	0.03 ± 0.01	0.03 ± 0.01
15	MIC	0.008 ± 0.0006	0.015 ± 0.003	0.008 ± 0.0006	0.008 ± 0.0006	0.008 ± 0.0006	0.008 ± 0.0006	0.008 ± 0.0006
	MFC	0.015 ± 0.003	0.03 ± 0.01	0.015 ± 0.003	0.015 ± 0.003	0.015 ± 0.003	0.015 ± 0.003	0.015 ± 0.003
16	MIC	0.015 ± 0.003	0.015 ± 0.003	0.015 ± 0.003	0.015 ± 0.003	0.015 ± 0.003	0.008 ± 0.0006	0.015 ± 0.003
	MFC	0.03 ± 0.01	0.03 ± 0.01	0.03 ± 0.01	0.03 ± 0.01	0.03 ± 0.01	0.015 ± 0.003	0.03 ± 0.01
17	MIC	0.008 ± 0.0006	0.06 ± 0.006	0.022 ± 0.005	0.015 ± 0.003	0.015 ± 0.003	0.11 ± 0.01	0.03 ± 0.01
	MFC	0.015 ± 0.003	0.12 ± 0.04	0.015 ± 0.003	0.03 ± 0.01	0.03 ± 0.01	0.015 ± 0.003	0.06 ± 0.006
Bifonazole	MIC	0.15 ± 0.05	0.15 ± 0.05	0.15 ± 0.05	0.10 ± 0.002	0.20 ± 0.01	0.15 ± 0.05	0.10 ± 0.009

	MFC	0.20 ± 0.01	0.20 ± 0.01	0.20 ± 0.01	0.20 ± 0.01	0.25 ± 0.05	0.20 ± 0.01	0.20 ± 0.01
Ketoconazole	MIC	0.25 ± 0.05	0.20 ± 0.01	0.20 ± 0.01	0.20 ± 0.01	2.50 ± 0.3	1.00 ± 0.1	0.20 ± 0.01
	MFC	0.50 ± 0.006	0.50 ± 0.001	0.50 ± 0.004	0.50 ± 0.002	3.50 ± 0.03	1.50 ± 0.09	0.30 ± 0.01

A.v.—A. versicolor, A.f.—A. fumigatus, A.n.—A. niger, A.o.—A. ochraceus, P.f.—P. funiculosum, T.v.—T. viride, P.v.c.—P. cyclpoium var verucosum, P.o.—P. ochrochloron

The activity of the tested compounds is ranked as follows: 15 > 3 > 16 > 10 > 7 > 6 > 2 > 5 > 11 > 9 > 13 > 4 > 12 > 17 > 14 > 1 > 8. Compound 15 exhibited the most potent antifungal activity, with MIC/MFC values ranging from 0.008–0.015/0.015–0.03 mg/mL, while compound 8 showed the weakest antifungal activity. However, the antibacterial activity showed an opposite trend, with compound 8 being the most active, while compound 15 was among the least effective. Some compounds displayed remarkable antifungal potency, surpassing the reference drugs. For instance, compound 1 demonstrated significant antifungal activity against *P. ochramensis* (MIC = 0.004 mg/mL), and compounds 3, 5, 7, and 10 were notably effective against *T. viride*. Moreover, compounds 10 and 9 exhibited comparable strong activity against *A. ochraceus.* A majority of the compounds showed strong activity against *A. ochraceus* (MIC = 0.008 mg/mL), with compounds 1, 2, 4–8, and 11 being particularly effective. Compounds 4, 6, 9, 11, 12, 15, and 16 also demonstrated excellent activity against *T. viride*, while compounds 6, 7, 10, and 15 were highly active against *P. ochramensis*. Compounds 3, 7, 10, and 15 displayed good activity against *A. niger* and *P. funiculosum.* Additionally, compound 15 exhibited potent activity against *P. cyclopium var verucosum*, as well as *A. fumigatus*, which is one of the most resistant fungal strains. Among all fungi tested, *T. viride* was the most susceptible.

The structure–activity relationship (SAR) analysis revealed that the methyl group on the nitrogen of the 2-thioxothiazolidin-4-one ring in compound 15 played a key role in enhancing antifungal activity. Substituting this methyl group with 4-hydroxybenzene (compound 3) or removing the fluorine from the indole ring slightly reduced the antifungal activity. Replacing the methyl group with morpholine in compound 16 decreased activity further, although it remained among the top three most active compounds. In contrast, the removal of the fluorine atom in compound 6 placed it lower in the activity ranking. On the other hand, introducing 3-methylbutanoic acid as a substituent on the nitrogen of the 2-thioxothiazolidin-4-one moiety (compound 8) significantly impaired antifungal activity, although compound 8 showed the highest antibacterial activity. These findings emphasize that both the substituent on the 2-thioxothiazolidin-4-one and the indole ring impact the antifungal and antibacterial activities.

Docking studies

Docking to Antibacterial Targets

To explore the potential mechanisms behind the antibacterial activity of the compounds, docking studies were performed with enzymes involved in common antibacterial mechanisms. The selected targets included *E. coli* DNA gyrase, thymidylate kinase, *E. coli* primase, and *E. coli* MurA and MurB enzymes. A lower Free Energy of Binding (FEB) indicates a stronger ligand-enzyme interaction. The docking results showed that the FEB values for all compounds were higher when binding to *E. coli* DNA gyrase, thymidylate kinase, *E. coli* primase, and *E. coli* MurA enzymes, compared to *E. coli* MurB (−7.54 to −10.88 kcal/mol). This suggests that *E. coli* MurB inhibition could be the primary mechanism of action for these compounds, as the binding affinity was consistent with their observed biological activity **(Table 4).**

Table 4. Molecular docking free binding energies (kcal/mol) to antibacterial targets.

Compound	E. coli MurB (2Q85)	E. coli Gyrase (1KZN)	Thymidylate Kinase (4QGG)	E. coli Primase (1DDE)	E. coli MurA (JV4T)	Residues Involved in H-Bond Formation in E. coli MurB
1	−9.82	−1.68	-	−5.63	−4.15	Arg213, Ser229
2	−10.04	-	-	−5.23	−3.17	Arg158, Ser229
3	−9.53	−2.55	−1.28	−6.27	−4.63	Arg213, Ser229

4	−7.90	-	-	−4.63	−5.10	Arg158, Arg213
5	−8.97	-	-	−5.20	−3.51	Arg213, Ser229
6	−7.68	-	−1.39	−4.82	−4.15	Arg213
7	−9.14	-	-	−6.12	−4.38	Arg158, Ser229
8	−10.88	−2.85	-	−5.92	−5.37	Ser50, Ser229
9	−8.11	-	-	−5.37	−4.12	Ser50, Arg158
10	−7.54	-	-	−5.42	−5.47	Ser50
11	−10.46	−3.47	−2.61	−6.20	−5.21	Ser116, Ser229
12	−9.56	−2.51	-	−5.73	−3.50	Ser229
13	−8.55	-	-	−5.14	−4.39	Ser229
14	−8.42	-	−1.29	−5.32	−4.26	Ser229
15	−7.60	-	−2.57	−5.18	−3.94	Arg213
16	−8.30	-	-	−4.92	−5.28	Ser229
17	−9.46	-	-	−5.16	−4.36	Arg158, Ser229

The most active compound, 8, showed two important hydrogen bond interactions in the docking pose with the E. coli MurB enzyme. One is between the carbonyl group's oxygen atom and the hydrogen from the Ser229 side chain (3.11 Å), while the other bond involves the sulfur of the thiazolidinone group and Ser50 (3.64 Å). In addition, hydrophobic interactions with residues such as Val52, Arg159, and Ile110 were observed, which help stabilize the ligand-enzyme complex **(Figure 4).** The hydrogen bond with Ser229 is particularly important for the inhibitory effect of this compound, as Ser229 plays a role in proton transfer during peptidoglycan synthesis [59]. Similar hydrogen bond interactions with Ser229 were seen for most compounds **(Table 4).**

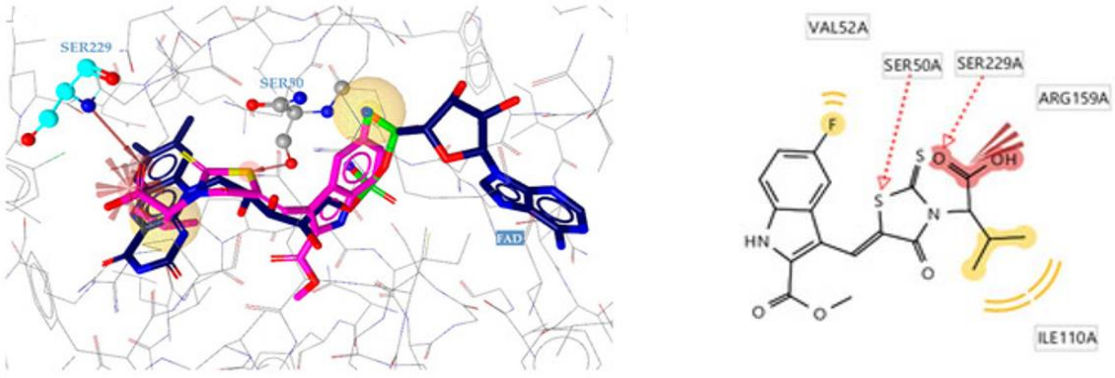

a) b)

Figure 4. (a) Alignment of compound 8 (magenta) and FAD (blue) within E. coli MurB. (b) The binding pose of the most effective compound 8 in E. coli MurB, with red dashed lines illustrating hydrogen bonds and yellow spheres indicating hydrophobic contacts.

In-depth examination of the binding poses for the most potent compounds revealed that they interact with MurB in a manner akin to FAD, occupying the enzyme's active site similarly and forming contacts with identical key residues, including Ser50, Arg213, Arg158, and Ser229 **(Figure 4a)**. This similarity likely accounts for their strong inhibitory effects, which were comparable to those of ampicillin.

Docking studies on antifungal targets

The synthesized compounds, along with the standard antifungal agent ketoconazole, were subjected to molecular docking against lanosterol 14α-demethylase from C. albicans and DNA topoisomerase IV **(Table 5)** to investigate potential mechanisms underlying their antifungal properties.

Table 5. Binding free energies (kcal/mol) from molecular docking against antifungal targets.

Compound	Estimated Binding Energy for CYP51 of C. albicans (5V5Z) (kcal/mol)	Estimated Binding Energy for DNA TopoIV (1S16) (kcal/mol)	Residues Involved in Aromatic Interactions	Residues Involved in Hydrophobic Interactions	Residues Involved in Hydrogen Bonding	Nature of Interactions with Heme (HEM601)
1	−7.54	−3.69	-	Tyr118, Thr311, Phe380, Met508, Hem601	-	Hydrophobic
2	−9.70	−3.18	Tyr118	Tyr118, Leu300, Ile304, Thr311, Hem601	Tyr132	Hydrophobic
3	−12.34	−3.25	Hem601	Tyr118, Ile131, Ile304, Hem601	Tyr132	Hydrophobic, aromatic, Fe coordination
4	−8.70	−2.66	Tyr118, Hem601	Tyr118, Leu300, Thr311, Leu376, Phe380, Met508, Hem601	-	Hydrophobic, aromatic
5	−9.34	−4.25	Tyr118	Tyr118, Leu376, Met508, Hem601	Tyr118	Hydrophobic
6	−9.65	−3.14	Tyr118	Tyr118, Tyr122, Thr311, Leu376, Phe380, Hem601	Tyr64	Hydrophobic
7	−9.82	−4.17	Hem601	Tyr118, Leu121, Thr311, Phe380, Met508, Hem601	Tyr132	Hydrophobic, aromatic
8	−7.11	−2.59	-	Tyr118, Leu376, Met508, Hem601	-	Hydrophobic
9	−9.54	−4.39	-	Tyr118, Phe380, Met508, Hem601	Tyr132	Hydrophobic
10	−10.11	−2.67	Tyr118, Hem601	Tyr118, Leu300, Thr311, Met508, Hem601	Tyr64	Hydrophobic, aromatic
11	−9.31	−2.73	Hem601	Leu300, Met508, Hem601	Tyr118	Hydrophobic, aromatic
12	−8.62	−4.37	Tyr122, Hem601	Tyr118, Tyr122, Thr311, Met508, Hem601	-	Hydrophobic, aromatic
13	−8.81	−3.56	Tyr118	Tyr118, Tyr122, Thr311, Leu376, Phe380, Hem601	-	Hydrophobic
14	−7.64	−3.28	-	Tyr118, Thr311, Leu376, Met508, Hem601	-	Hydrophobic
15	−12.95	−3.10	Hem601	Ile131, Leu300, Ile304, Hem601	Thr311	Hydrophobic, aromatic, Fe coordination
16	−10.26	−2.67	Hem601	Tyr118, Tyr122, Leu300, Ile304, Hem601	Tyr132	Hydrophobic, aromatic
17	−7.96	−2.57	Tyr118, Hem601	Tyr118, Tyr122, Thr311, Leu376, Met508, Hem601	-	Hydrophobic, aromatic
Ketoconazole	−8.23	-	Hem601	Tyr118, Ile131, Tyr132, Leu300, Ile304, Leu376, Met508, Hem601	Tyr64	Hydrophobic, aromatic

Docking studies revealed that both a novel Compound 15 and the standard drug, ketoconazole, bind to the CYP51Ca enzyme in a similar manner around the heme group. A key difference is that Compound 15 forms a more stable complex by directly interacting with the iron (Fe) atom of the heme, which ketoconazole also does, but less stably. Compound 15 also establishes a specific hydrogen bond via its CO_2 group with the Thr311 residue, and engages in several hydrophobic and aromatic interactions (with residues like Ile304, Leu300, and Ile131) via its benzene ring. This stronger, more stable binding of Compound 15 is suggested to be the reason for its superior antifungal activity compared to ketoconazole.

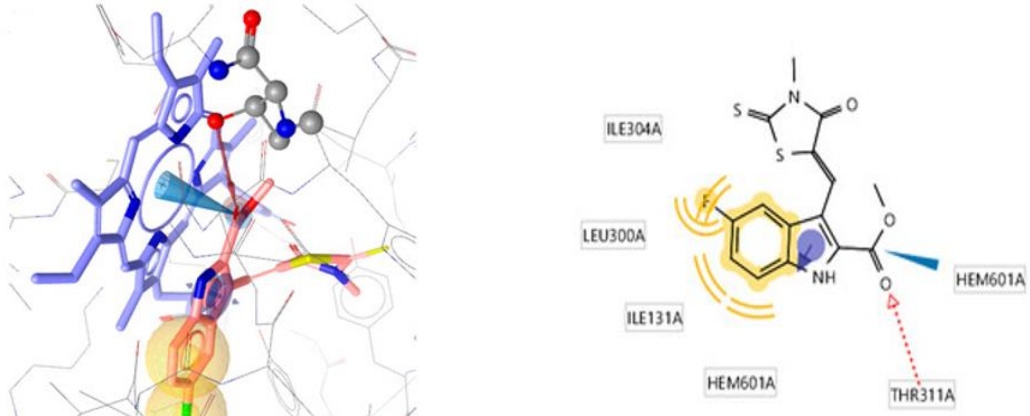

a) b)

Figure 5. Binding pose of the most effective compound 15 in the lanosterol 14α-demethylase (CYP51ca) of *C. albicans*. (a) Three-dimensional view of compound 15. (b) Two-dimensional illustration, where red dashed lines represent hydrogen bonds, yellow spheres highlight hydrophobic interactions and blue arrows indicate aromatic interactions.

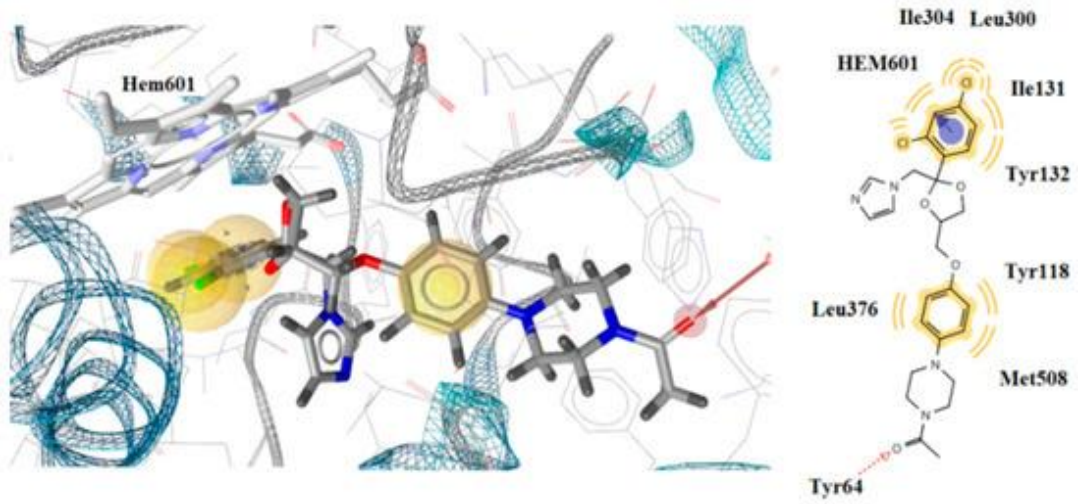

Figure 6. Docking position of ketoconazole in the lanosterol 14α-demethylase (CYP51ca) of *C. albicans*.

Bioavailability and drug-likeness

The evaluation of Drug-Likeness and Bioavailability for the tested molecules is presented in **Table 6**. Predictive models suggest that the majority of compounds achieved a bioavailability score of approximately 0.55. A subset of compounds, namely 2, 9, 12, 14, and 17**,** showed a significantly different result, registering a score of only 0.11. Based on the visual assessment provided by the BOILED-Egg diagram **(Figure 7a),** it is anticipated that all tested molecules will exhibit absorption levels ranging from moderate to high within the gastrointestinal (GI) system. Specifically, compounds 5, 6, 7, 15, and 16 are expected to be absorbed passively across the GI tract lining. Importantly, the analysis indicates that none of these compounds are predicted to passively diffuse into the

central nervous system (i.e., permeate the blood–brain barrier). Furthermore, every compound adhered to the established criteria of Lipinski's rule of five**.** Half of the set possessed a Topological Polar Surface Area (TPSA) value below 140 A˚2140 \text{Å}^2140 A˚2, which is generally associated with robust oral availability. The overall drug-likeness metrics for all compounds were moderate, spanning from −0.95-0.95−0.95 **to** 0.380.380.38. This moderate range may be influenced by the higher TPSA values found and the structural lack of a basic functionality linked to the nitrogen atom of the rhodanine ring system. The most favorable outcome from the *in silico* modeling belonged to compound 5**,** which incorporates a basic propyl-morpholine group, resulting in the highest drug-likeness rating of 0.24 **(Figure 7 and Table 6).**

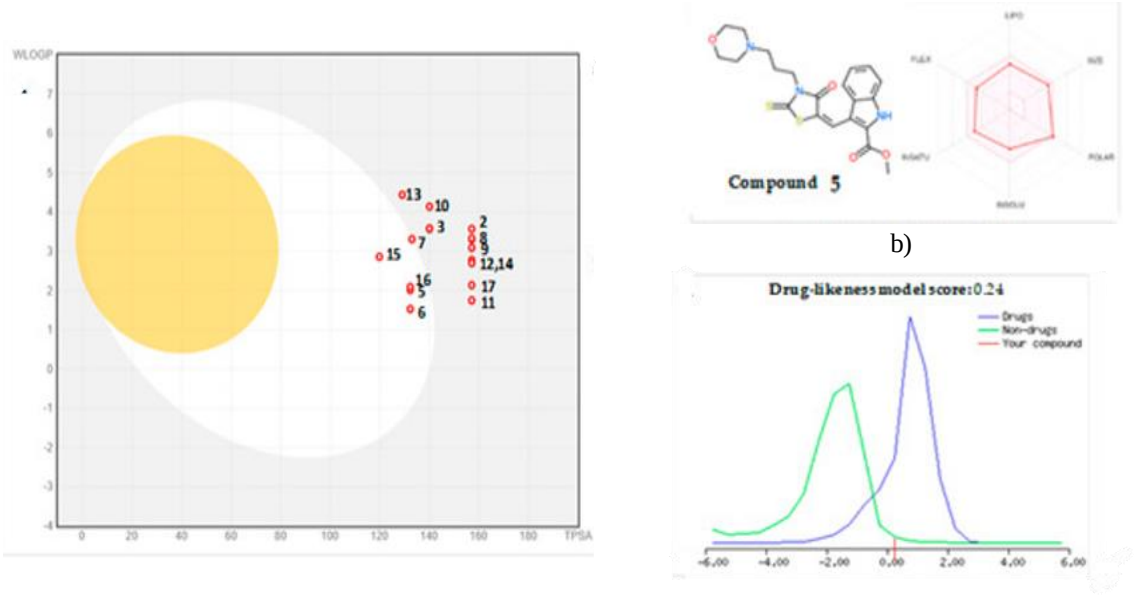

a) b) c)

Figure 7. presents' three complementary visualizations: (a) A graphic depicting a boiled egg, (b) A radar chart illustrating the bioavailability metrics for compound 5, and (c) The drug-likeness assessment profile**.** Within the bioavailability radar chart, the area shaded in pink demarcates the optimal criteria for each characteristic required to ensure favorable oral absorption: Lipophilicity (LIPO) must correspond to an XLOGP3 value ranging from −0.7 to +5.0; Molecular weight (SIZE) is stipulated to be within the 150 to 500 g/mol range; Polarity (POLAR) necessitates a TPSA reading between 20 and 130 $A^{\circ 2}$; Solubility (INSOLU) should have a log S value not exceeding −6; Saturation (INSATU) requires that a minimum of 0.25 fraction of its carbon atoms exhibit sp^3 hybridization; and Flexibility (FLEX) is constrained to a maximum of nine bonds capable of rotation.

Table 6. contains the calculated predictions concerning the drug-likeness properties for all the compounds that were evaluated.

Compound	Molecular Weight (MW)	HBDs (≤5)	HBAs (≤10)	Lipophilicity (ClogP) (≤5)	TPSA (≤140)	Rotatable Bonds (RBs) (≤10)	Bioavailability Score	Lipinski Violations	Drug-Likeness Score
1	432.51	2	5	3.30	157.09	9	0.55	0	−0.14
2	438.48	2	5	3.45	157.09	5	0.11	0	−0.64
3	410.47	2	4	3.46	140.02	4	0.55	0	−0.78
4	410.47	2	4	3.47	140.02	4	0.55	0	−0.81
5	445.56	1	5	2.86	132.26	7	0.55	0	+0.24
6	403.48	1	5	2.48	132.26	4	0.55	0	−0.38
7	398.46	1	4	3.28	132.93	5	0.55	0	−0.69

8	436.48	2	6	3.31	157.09	6	0.55	0	−0.70
9	422.45	2	6	2.99	157.09	7	0.11	0	−0.37
10	428.46	2	5	3.78	140.02	4	0.55	0	−0.77
11	376.41	2	5	2.11	157.09	5	0.55	0	−0.71
12	418.49	2	5	3.02	157.09	6	0.11	0	−0.24
13	442.48	1	5	4.15	129.02	5	0.55	0	−0.95
14	408.42	2	6	2.65	157.09	6	0.11	0	−0.40
15	350.39	1	4	3.02	119.79	3	0.55	0	−0.15
16	421.47	1	6	2.79	132.26	4	0.55	0	−0.14
17	390.43	2	5	2.35	157.09	6	0.11	0	−0.59

[a] is Molecular weight; [b] denotes the count of hydrogen bond acceptors; [c] represents the number of hydrogen bond donors; [d] signifies the consensus logarithm of the partition coefficient (octanol/water), calculated as the average derived from five distinct methodologies (iLOGP, XLOGP3, WLOGP, MLOGP, SILICOS-IT); [e] is the count of rotatable bonds; and [f] is the topological polar surface area, expressed in A˚

Admet properties

The ADMET profile for all compounds was evaluated utilizing ADMET Predictor software, version 10.4, developed by Simulation Plus [1,2,3,4,5,6,7,8,9,10,11,12,13,14,15,16,17,18,19,20,21,22,23,24,25,26,27,28,29,30,31,32,33,34,35,36,37,38,39,40,41,42,43,44,45,46,47,48,49,50,51,52,53]. We observed that compounds designated as 1, 8, 9, 11, 12, 14, and 17 exhibit preferred characteristics pertaining to distribution and, critically, absorption **(Table 7).** Despite the permeability indices being moderate due to the presence of a carboxylate functional group, these specific compounds displayed a reduced propensity for crossing the blood-brain barrier (indicated by lower logBB values) alongside acceptable water and salt solubility at the physiological blood pH of 7.4. Furthermore, based on favorable solubility metrics in the fed-state simulated intestinal fluid (FeSSIF), it is our assessment that these compounds would likely be well absorbed via the oral route following food intake in the small intestine. Conversely, when contrasted with the other molecules in this group (such as neutral or basic counterparts), these compounds show low fraction unbound values, remaining under 6.0%. Nonetheless, the predicted values for the volume of distribution (Vd) and the blood-to-plasma ratio (RBP) in human subjects were determined to be acceptable for every compound in this series.

Table 7. Summarizes the absorption and distribution characteristics evaluated for the compounds numbered 1 through 17.

Peff (a)	**MDCK (b)**	**Sw (c)**	**SpH (d)**	**FaSSGF (e)**	**FaSSIF (f)**	**FeSSIF (g)**	**BBB (h)**	**LogBBB (i)**	**fu% (j)**	**Vd (k)**	**Absorption Risk**
1.642	18.188	23	10.009	0.009	0.067	0.160	−1.231	4.588	0.328	0.661	Low (59%)
2.232	112.633	5	1.295	0.008	0.040	0.115	−0.793	4.446	0.244	0.692	Low (66%)
2.491	160.415	2	0.002	0.026	0.010	0.155	−0.071	4.548	0.691	0.738	High (89%)
2.439	192.624	2	0.002	0.026	0.008	0.111	−0.127	4.449	0.742	0.737	High (88%)
1.979	244.487	30	0.049	0.914	0.031	0.089	−0.006	9.925	1.232	0.748	High (99%)
2.608	289.456	8	0.008	0.124	0.071	0.197	−0.130	9.631	1.097	0.767	High (99%)
2.846	695.382	2	0.002	0.013	0.013	0.159	−0.393	5.233	0.780	0.744	High (94%)
1.713	20.994	28	6.904	0.009	0.035	0.381	−0.964	5.525	0.325	0.680	Low (84%)
1.824	11.524	37	14.568	0.014	0.090	0.207	−1.151	5.491	0.328	0.677	Low (66%)
2.552	238.505	2	0.002	0.024	0.005	0.104	−0.046	4.722	0.746	0.741	High (77%)
1.557	18.324	37	7.429	0.017	0.092	0.380	−1.047	5.954	0.313	0.684	Low (74%)
1.624	16.857	29	7.179	0.010	0.051	0.308	−1.056	5.402	0.327	0.677	Low (84%)
3.755	512.700	1	0.001	0.018	0.006	0.085	0.129	4.768	0.861	0.731	High (96%)
1.864	39.838	38	13.699	0.014	0.178	0.322	−0.997	5.963	0.313	0.683	Low (90%)
3.536	572.262	4	0.004	0.099	0.018	0.211	0.137	9.910	0.779	0.783	High (99%)

3.229	352.377	8	0.008	0.122	0.061	0.169	−0.037	10.236	1.141	0.769	High (99%)
1.652	29.583	38	13.731	0.015	0.236	0.260	−1.085	5.838	0.314	0.680	Low (84%)

[a.] Human jejunal permeability (10^4 cm/s); [b.] MDCK Transwell permeability (10^7 cm/s); [c.] Water solubility (μg/mL); [d.] Solubility in water at pH 7.4 (mg/mL); [e.] Solubility in fasted-state simulated gastric fluid (mg/mL); [f.] Solubility in fasted-state simulated intestinal fluid (mg/mL); [g.] Solubility in fed-state simulated intestinal fluid (mg/mL); [h.] Potential for crossing the blood-brain barrier; [i.] Logarithmic value of the brain-to-blood partition ratio; [j.] Human fraction unbound (%); [k.] Volume of distribution in steady state in humans (L/kg); [l.] Blood-to-plasma ratio in humans.

It is predicted that metabolism is the primary clearance route for all compounds, with a 74–99% probability, rather than hepatic uptake or renal elimination, which both have a 99% likelihood. Given this, a detailed in silico analysis of cytochrome P450-mediated metabolism for our compounds was performed **(Table 8).** The analysis revealed that the presence of various groups attached to the nitrogen atom in the rhodanine scaffold significantly affects the metabolism of the compounds. For the most well-absorbed compounds, such as 8 and 12, high clearance through the CYP2C9 isoenzyme was observed, indicating a CYP risk above zero. Conversely, compounds 1, 9, 11, 14, and 17 showed no CYP-related risks, marking them as having optimal metabolic properties for further investigation.

Furthermore, compounds 1, 2, 8–12, 14, and 17 are not expected to be substrates for CYP2E1 (67–87%), while compounds 3–7, 13, 15, and 16 are anticipated to be good CYP2E1 substrates. In addition, the majority of the compounds are predicted to inhibit the CYP3A4 isoenzyme (33–80%), except for compounds 1, 2, 8, 11, and 12, which show an inhibition range of 71–75%. Despite these variations in metabolic pathways, all compounds are likely to inhibit CYP1A2 (68–97%), though they do not inhibit CYP2C9 (62–95%), CYP2C19 (94–99%), or CYP2D6 (95%).

According to the findings in **Table 8**, the main metabolizing enzymes for compounds 1, 9, 11, 14, and 17 are predicted to be CYP2C9 and CYP2C19, responsible for over 90% of the metabolism. Additionally, all compounds are likely to be metabolized by CYP2C8 (70–91%) instead of CYP2A6 (67–99%) or CYP2B6 (57–98%). Glucuronidation by UDP-glucuronosyltransferases 1A3 and 1A9 is also anticipated for these compounds. Lastly, compounds 1, 9, 11, 14, and 17 are expected to show the most promising metabolism profiles based on their low intrinsic clearance values in relation to cytochrome P450 metabolism (CYP-CLint) and hepatic clearance in humans (HEP-CLint).

Table 8. Metabolic Profiles of Compounds 1–17.

Compound	CYP1A2 Inhibition	CYP1A2 Substrate Km	CYP3A4 Inhibition	CYP3A4 Substrate Km	CYP2D6 Inhibition	CYP2D6 Substrate Km	CYP2C9 Inhibition	CYP2C9 Substrate Km	CYP2C19 Inhibition	CYP2C19 Substrate Km	CYP-CLint (μL/min/mg)	HEP-CLint (mL/min/kg)	UGTs Substrates	CYP Risk
1	No	Non-Substrate	No	Non-Substrate	No	Non-Substrate	No	86.146	No	24.703	6.568	11.362	1A3, 1A9	0.000
2	No	23.682	No	Non-Substrate	No	Non-Substrate	No	8.127	No	39.264	100.398	16.359	1A8, 1A9, 1A10	2.000
3	No	30.916	Yes	Non-Substrate	No	127.051	No	14.403	No	29.495	65.013	71.146	1A1, 1A8, 1A9, 1A10, 2B15	2.372
4	No	29.485	Yes	Non-Substrate	No	204.398	No	8.423	No	93.004	80.365	89.557	1A1, 1A8, 1A9, 1A10, 2B15	2.985

5	No	18.129	Yes	22.767	No	13.006	No	83.216	No	20.465	78.710	23.739	1A4, 1A9	1.147
6	No	7.486	Yes	31.235	No	28.012	No	87.569	No	44.972	101.603	18.418	Non-Substrate	1.000
7	No	26.192	Yes	21.943	No	38.409	No	15.906	No	4.882	89.261	21.857	1A9	0.981
8	No	Non-Substrate	No	Non-Substrate	No	Non-Substrate	No	20.918	No	203.738	19.358	7.088	1A3, 1A8, 1A9, 1A10	0.935
9	No	Non-Substrate	Yes	Non-Substrate	No	Non-Substrate	No	123.319	No	16.370	6.868	8.300	1A3, 1A9	0.000
10	No	34.151	Yes	Non-Substrate	No	255.204	No	7.744	No	94.454	131.921	93.639	1A1, 1A8, 1A9, 1A10, 2B15	3.000
11	No	Non-Substrate	No	Non-Substrate	No	Non-Substrate	No	36.930	No	220.331	9.918	5.080	1A3, 1A8, 1A9	0.000
12	No	Non-Substrate	No	Non-Substrate	No	Non-Substrate	No	25.953	No	199.456	12.348	6.689	1A3, 1A8, 1A9	0.234
13	No	3.514	Yes	11.550	No	27.176	No	15.364	No	66.722	259.955	80.554	1A1, 1A9	3.228
14	No	Non-Substrate	Yes	Non-Substrate	No	Non-Substrate	No	96.500	No	5.165	13.286	6.370	1A3, 1A9	0.000
15	No	20.385	Yes	130.324	No	91.889	No	167.240	No	60.458	57.430	21.782	1A1, 1A9	0.740
16	No	9.212	Yes	24.123	No	32.873	No	64.353	No	48.228	102.341	18.506	1A8, 1A9	1.055
17	No	Non-Substrate	Yes	Non-Substrate	No	Non-Substrate	No	100.364	No	4.815	10.276	5.966	1A3, 1A9	0.000

[a]. Total intrinsic clearance mediated by human cytochrome P-450, calculated by summing the clearances of CYP1A2, CYP2C9, CYP2C19, CYP2D6, and CYP3A4; [b]. Intrinsic clearance in human hepatocytes (μL/min/10^6 cells);
[c]. Potential substrates for UDP-glucuronosyltransferase (UGT) isoenzymes.

We have also simulated the metabolic pathways of the most potent compounds with favorable metabolic profiles, specifically compounds 1 **(Figure 8)** and 11 **(Figure 9)**. Both compounds undergo two primary metabolic processes: oxidation and demethylation. In particular, carboxylic acid derivatives resulting from demethylation represent 10% and 6% of the metabolic products for compounds 1 and 11, respectively. CYP2C9 and CYP2C19 are mainly responsible for transforming the free ester groups into carboxylic acid derivatives with similar yields. During the oxidation process, 6-hydroxy-indole derivatives are formed, comprising approximately 27% and 22% of the metabolism for compounds 1 and 11, respectively. Moreover, CYP2C9 plays a significant role in the formation of sulfone derivatives, leading to M4 in 27% of compound 1's metabolism, while M2 forms in 18% of compound 11's metabolism. Interestingly, the major metabolites for both compounds are identified as 2,4-thiazolidinones (1-M3 and 11-M1), with remarkable formation rates of 36% and 53%, respectively. Additionally, CYP2C8 impacts the metabolism of compound 1 by cleaving the acidic tail from the rhodanine nitrogen atom, producing a metabolite, 6-oxohexanoic acid. This process is unique to compound 1 and does not occur in compound 11, which contains a shorter acetic acid chain. Finally, after simulating at least three cycles of metabolism, all metabolites of compounds 1 and 11 were predicted to be non-toxic.

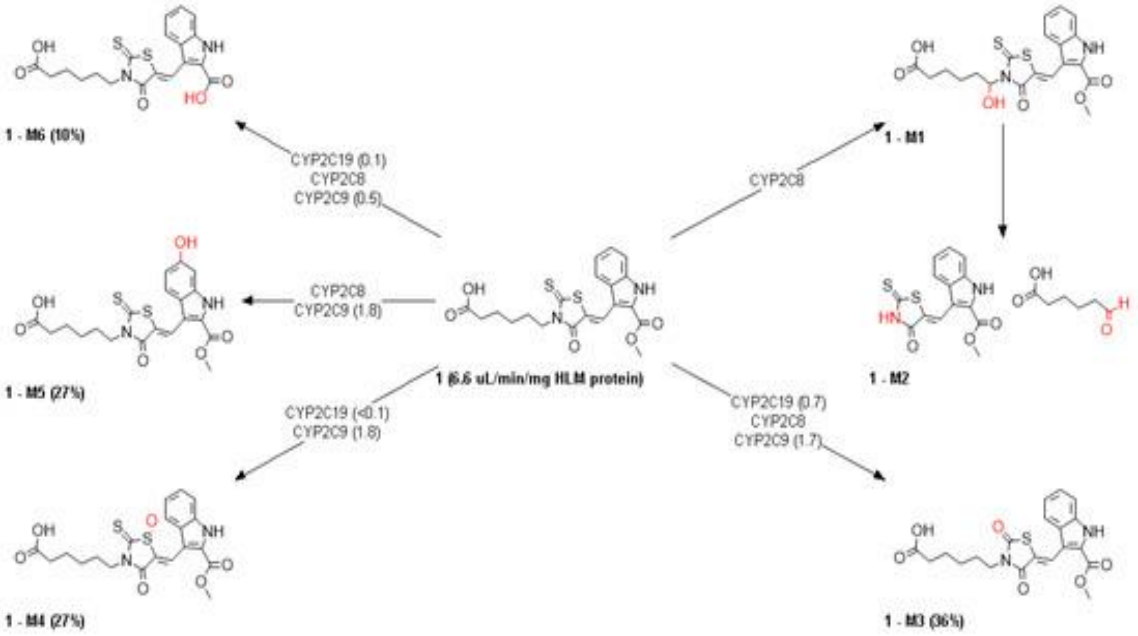

Figure 8. Metabolism of compound **1**.

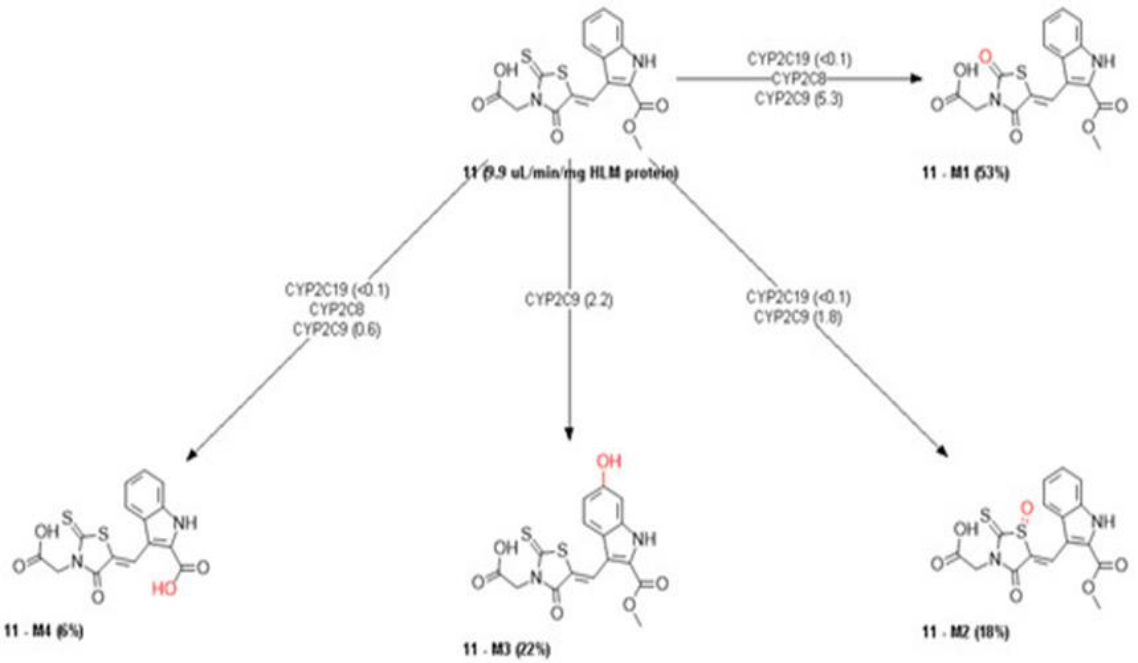

Figure 9. Metabolism of compound **11**.

We conducted a detailed investigation into the potential of our compounds to act as substrates or inhibitors for specific human transporters, which are crucial for pharmacokinetic properties, particularly in distribution and excretion **(Table 9).** The ADMET Predictor software analysis indicated that all compounds, except for compound 12, are effective substrates for P-glycoprotein (90–99%) and breast cancer resistance protein (BCRP) (62–95%). Additionally, the compounds were found not to inhibit BCRP (69–97%). Regarding P-glycoprotein inhibition, most of the compounds are not inhibitors, with the exception of compounds 2–7, 10, 13, and 16. Furthermore, the bile salt export pump (BSEP), which is primarily expressed in the liver and is closely related to hepatotoxicity, was also studied. Inhibition of BSEP can lead to the accumulation of bile salts in the liver, potentially resulting in cholestasis and drug-induced liver injury (DILI) [60]. For the majority of the compounds tested, no significant inhibition of BSEP was predicted (≥52%), suggesting a low risk of hepatotoxicity.

Table 9. Studies on selected transporters for the examined compounds 1–17.

Compound	P-glycoprotein Inhibitor (Pgp Inh.)	P-glycoprotein Substrate (Pgp Sub.)	BCRP Inhibitor (BCRP Inh.)	BCRP Substrate (BCRP Sub.)	Bile Salt Export Pump Inhibitor (BSEP Inh.)
1	No (49%)	Yes	No	Yes	No
2	Yes (62%)	Yes	No	Yes	No
3	Yes (97%)	Yes	No	Yes	No
4	Yes (97%)	Yes	No	Yes	No
5	Yes (88%)	Yes	No	Yes	No
6	Yes (60%)	Yes	No	Yes	No
7	Yes (97%)	Yes	No	Yes	No
8	No (93%)	Yes	No	Yes	No
9	No (49%)	Yes	No	Yes	No
10	Yes (97%)	Yes	No	Yes	No
11	No (93%)	Yes	No	Yes	No
12	No (93%)	Yes	No	No	No
13	Yes (97%)	Yes	No	Yes	No
14	No (68%)	Yes	No	Yes	No
15	No (46%)	Yes	No	Yes	No
16	Yes (57%)	Yes	No	Yes	No
17	No (78%)	Yes	No	Yes	No

Cytotoxicity

To assess cytotoxicity, compounds 1, 2, 8, and 11 were selected for testing in the human fetal lung fibroblast MRC-5 cell line. The compounds were tested across three concentrations: 1×10^{-7} M (0.1 µM), 1×10^{-6} M (1 µM), and 1×10^{-5} M (10 µM). As illustrated in **Figure 10**, after 48 hours of exposure, none of the compounds demonstrated significant cytotoxic effects within the tested concentration range, with cell viability remaining ≥91% when compared to the untreated control. Among the compounds, only compound 11 showed a marginal decrease in cellular viability at concentrations of 1 µM and 10 µM, with a viability of 91.0%. In contrast, compounds 1, 2, and 8 did not produce any statistically significant changes in cell viability relative to the control. Overall, the results suggest that, at the concentrations tested, these compounds do not exhibit cytotoxicity in human MRC-5 cells.

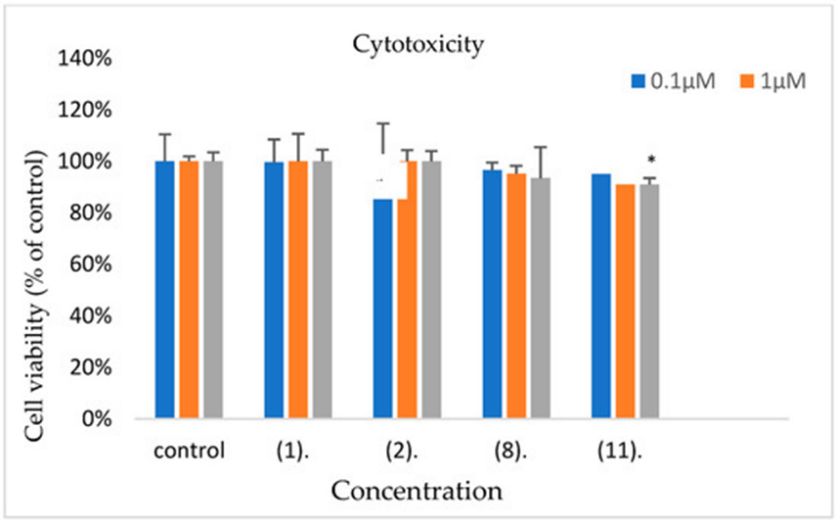

Figure 10. Percentage cell viability of human lung fibroblast MRC-5 cells following 48-hour incubation with varying doses of selected compounds (1, 2, 8, and 11). Results are shown as average values ± SD derived from three separate experiments, each conducted in triplicate. Concentrations exhibiting statistically

significant deviations from the untreated control are marked with an asterisk (*), where significance is defined as $p < 0.05$.

Conclusion

We successfully designed, synthesized, and tested seventeen derivatives of (Z)-methyl 3-((4-oxo-2-thioxothiazolidin-5-ylidene) methyl)-1H-indole-2-carboxylate (labeled 1–17) through both computational predictions and laboratory experiments for activity against various bacteria (Gram-positive and Gram-negative) and fungi.

All synthesized molecules showed superior antibacterial performance compared to the standards ampicillin and streptomycin across the bacterial panel. The strain most vulnerable was En. cloacae, while E. coli displayed the highest resistance, with M. flavus next.

For antifungal properties, the derivatives demonstrated potent to highly effective inhibition of all tested fungi, exceeding the activities of ketoconazole and bifonazole. Several compounds were especially strong against A. ochraceus and T. viride, the latter proving most susceptible overall. In contrast, A. fumigatus was the toughest to inhibit among the filamentous fungi.

Differences in how bacterial and fungal growth was affected highlight potential variations in action mechanisms tied to substituent groups, or possible microbial adaptations/metabolic resistance to certain derivatives.

Docking results against targets like DNA gyrase, thymidylate kinase, and E. coli MurB pointed to MurB as a key site for antibacterial effects. Similarly, interactions with CYP51 (14α-lanosterol demethylase) and tetrahydrofolate reductase in Candida albicans suggested CYP51 involvement in antifungal mechanisms.

Drug-likeness predictions yielded scores from −0.89 to +0.24, with no breaches of Lipinski's rules. Six compounds appeared suitable for oral uptake based on TPSA under 140 Å². Using Simulation Plus' ADMET Predictor 10.4, compounds 1, 8, 9, 11, 12, 14, and 17 stood out for excellent absorption and distribution potential.

For the top performers 1 and 11 with favorable metabolism predictions, likely biotransformations included conversion of the rhodanine moiety to thiazolidinone and hydroxylation on the indole core. Tests on MRC-5 cells confirmed lack of toxicity for the series.

These molecules thus serve as valuable starting points for creating new, potent antimicrobial drugs with a safe profile.

Acknowledgments: None

Conflict of Interest: None

Financial Support: None

Ethics Statement: None

References

1. Chopra I, Schofield C, Everett M, O'Neill A, Miller K, Wilcox M, et al. Treatment of health-care-associated infections caused by gram-negative bacteria: A consensus statement. Lancet Infect Dis. 2008;8:133-9.
2. Overbye KM, Barrett JF. Antibiotics: Where did we go wrong? Drug Discov Today. 2005;10:45-52.
3. Baker AW, Maziarz EK, Arnold CJ, Johnson MD, Workman AD, Reynolds JM, et al. Invasive fungal infection after lung transplantation: Epidemiology in the setting of antifungal prophylaxis. Clin Infect Dis. 2020;70:30-9.
4. Sayed M, Kamal El-Dean AMK, Ahmed M, Hassanien R. Synthesis of some heterocyclic compounds derived from indole as antimicrobial agents. Synth Commun. 2018;48:413-21.
5. Roszczenko P, Holota S, Szewczyk OK, Dudchak R, Bielawski K, Bielawska A, et al. 4-Thiazolidinone-bearing hybrid molecules in anticancer drug design. Int J Mol Sci. 2022;23:13135.
6. Horishny V, Kartsev V, Matiychuk V, Geronikaki A, Petrou A, Pogodin P, et al. 3-Amino-5-(indol-3-yl)methylene-4-oxo-2-thioxothiazolidine derivatives as antimicrobial agents: Synthesis, computational and biological evaluation. Pharmaceuticals (Basel). 2020;13:229.

7. Barakat A, Al-Najjar HJ, Al-Majid AM, Soliman SM, Mabkhot YN, Al-Agamy MHM, et al. Synthesis, molecular structure investigations and antimicrobial activity of 2-thioxothiazolidin-4-one derivatives. J Mol Struct. 2015;1081:519-29.
8. Cebeci YU, Karaoğlu ŞA. Quinolone-rhodanine hybrid compounds: Synthesis and biological evaluation as anti-bacterial agents. ChemistrySelect. 2022;7:e202201007.
9. Abusetta A, Alumairi J, Alkaabi MY, Al Ajeil R, Shkaidim AA, Akram D, et al. Design, synthesis, in vitro antibacterial activity, and docking studies of new rhodanine derivatives. Open J Med Chem. 2020;10:15-34.
10. Kumar AS, Kumar RA, Reddy EP, Satyanarayanaa V, Kashannab J, Reddy BJM, et al. Synthesis of novel 2-thioxothiazolidin-4-one and thiazolidine-2,4-dione derivatives as potential anticancer agents. Nat Prod Commun. 2018;13:589-91.
11. Manikala V, Rao MV. Synthesis, molecular docking and anticancer activity of novel (E)-5-((1-phenyl-1H-1,2,3-triazol-4-yl)methylene)-2-thioxothiazolidin-4-one analogues. Iran J Chem Chem Eng. 2021;40:1793-9.
12. Battula H, Bommi S, Bobde Y, Patel TT, Ghosh BB, Jayanty S. Distinct rhodamine B derivatives exhibiting dual effect of anticancer activity and fluorescence property. J Photochem Photobiol. 2021;6:100026.
13. Tintori C, Iovenitti G, Ceresola ER, Ferrarese R, Zamperini C, Brai A, et al. Rhodanine derivatives as potent anti-HIV and anti-HSV microbicides. PLoS One. 2018;13:e0198478.
14. Zhang Y, Xia L, Yuan Y, Li Q, Han L, Yang G, et al. Rhodanine derivative LJ001 inhibits TGEV and PDCoV replication in vitro. Virus Res. 2020;289:198167.
15. Khairul A, Kamar DA, Yin LJ, Liang CT, Fung GT, Avupati VR. Rhodanine scaffold: A review of antidiabetic potential and structure-activity relationships (SAR). Med Drug Discov. 2022;15:100131.
16. Toumi A, Boudriga S, Hamden K, Sobeh M, Cheurfa M, Askri M, et al. Synthesis, antidiabetic activity and molecular docking study of rhodanine-substitued spirooxindole pyrrolidine derivatives as novel α-amylase inhibitors. Bioorg Chem. 2021;106:104507.
17. Xu J, Wang TT, Yuan Q, Duan YT, Xu YJ, Lv PC, et al. Discovery and development of novel rhodanine derivatives targeting enoyl-acyl carrier protein reductase. Bioorg Med Chem. 2019;27:1509-16.
18. Previti S, Grasso S, Zappalà M, Ottanà R. Identification of 2-thioxoimidazolidin-4-one derivatives as novel noncovalent proteasome and immunoproteasome inhibitors. Bioorg Med Chem Lett. 2018;28:278-83.
19. Vitaku DT, Smith JTN. Analysis of the structural diversity, substitution patterns, and frequency of nitrogen heterocycles among U.S. FDA approved pharmaceuticals. J Med Chem. 2014;57:10257-74.
20. Dhiman A, Sharma R, Singh RK. Target-based anticancer indole derivatives and insight into structure-activity relationship: A mechanistic review update (2018-2021). Acta Pharm Sin B. 2022;12:3006-27.
21. Devi N, Kaur K, Biharee A, Jaitak V. Recent development in indole derivatives as anticancer agent: A mechanistic approach. Anticancer Agents Med Chem. 2021;21:1802-24.
22. Jia Y, Wen X, Gong Y, Wang X. Current scenario of indole derivatives with potential anti-drug-resistant cancer activity. Eur J Med Chem. 2020;200:112359.
23. Bhat MA, Al-Omar MA, Raish M, Ansari MA, Abuelizz HA, Bakheit AH, et al. Indole derivatives as cyclooxygenase inhibitors: Synthesis, biological evaluation and docking studies. Molecules. 2018;23:1250.
24. Kumari A, Singh RK. Synthesis, molecular docking and biological evaluation of N-substituted indole derivatives as potential anti-inflammatory and antioxidant agents. Chem Biodivers. 2022;19:e202200290.
25. Ji J, He H, Zhang X, Wu R, Gan L, Li D, et al. The in vitro and in vivo study of oleanolic acid indole derivatives as novel anti-inflammatory agents: Synthesis, biological evaluation, and mechanistic analysis. Bioorg Chem. 2021;113:104981.
26. Zhu Y, Zhao J, Luo L, Gao Y, Bao H, Li P, et al. Research progress of indole compound with potential antidiabetic activity. Eur J Med Chem. 2021;223:113665.
27. Taha M, Alrashedy AS, Almandil NB, Iqbal N, Anouar EH, Nawaz M, et al. Synthesis of indole derivatives as diabetics II inhibitors and enzymatic kinetics study of α-glucosidase and α-amylase along with their in-silico study. Int J Biol Macromol. 2021;190:301-18.
28. Dorababu A. Indole-A promising pharmacophore in recent antiviral drug discovery. RSC Med Chem. 2020;11:1335-53.
29. Sahin K. Investigation of novel indole-based HIV-1 protease inhibitors using virtual screening and text mining. J Biomol Struct Dyn. 2021;39:3638-48.

30. Cihan-Üstündağ G, Naesens L, Şatana D, Erköse-Genç GG, Mataracı-Kara E, Çapan G. Design, synthesis, antitubercular and antiviral properties of new spirocyclic indole derivatives. Monatsh Chem. 2019;150:1533-44.
31. Bajad NG, Singh SK, Singh SK, Singh TD, Singh M. Indole: A promising scaffold for the discovery and development of potential anti-tubercular agents. Curr Res Pharmacol Drug Discov. 2022;3:100119.
32. Porwal S, Gupta S, Chauhan PMS. gem-Dithioacetylated indole derivatives as novel antileishmanial agents. Bioorg Med Chem Lett. 2017;27:4643-6.
33. Tiwari S, Kirar S, Banerjee UC, Neerupudi KB, Singh S, Abdullah A, et al. Synthesis of N-substituted indole derivatives as potential antimicrobial and antileishmanial agents. Bioorg Chem. 2020;99:103787.
34. Elkamhawy A, Woo J, Nada H, Angeli A, Bedair TM, Supuran CT, et al. Identification of novel and potent indole-based benzenesulfonamides as selective human carbonic anhydrase II inhibitors: Design, synthesis, in vitro, and in silico studies. Int J Mol Sci. 2022;23:2540.
35. Asati V, Bhupal R, Bhattacharya S, Kaur K, Gupta GD, Pathak A, et al. Recent updates of indole derivatives as kinase inhibitors in the treatment of cancer. Anticancer Agents Med Chem. 2022;23:404-16.
36. Yuan W, Yu Z, Song W, Li Y, Fang Z, Zhu B, et al. Indole-core-based novel antibacterial agent targeting FtsZ. Infect Drug Resist. 2019;12:2283-96.
37. Al-Wabli RI, Alsulami MA, Bukhari SI, Moubaye NMS, Al-Mutairi MS, Attia MI, et al. Design, synthesis, and antimicrobial activity of certain new indole-1,2,4 triazole conjugates. Molecules. 2021;26:2292.
38. Tha S, Shakya S, Malla M, Aryal P. Prospects of indole derivatives as methyl transfer inhibitors: Antimicrobial resistance managers. BMC Pharm Toxicol. 2020;21:33-44.
39. Kaur H, Singh J, Narasimhan B. Indole hybridized diazenyl derivatives: Synthesis, antimicrobial activity, cytotoxicity evaluation and docking studies. BMC Chem. 2019;13:65-83.
40. Qin HL, Jing L, Fang WY, Rakesh KP. Indole-based derivatives as potential antibacterial activity against methicillin-resistant Staphylococcus aureus (MRSA). Eur J Med Chem. 2020;194:112245.
41. Horishny V, Geronikaki A, Kartsev V, Matiychuk V, Petrou A, Pogodin P, et al. Synthesis, biological evaluation and molecular docking studies of 5-indolylmethylen-4-oxo-2-thioxothiazolidine derivatives. Molecules. 2020;25:1964.
42. Michael GP, Chennaiah A, Klara H, Sven NH, Andrea V, Erik CB, et al. Importance of co-operative hydrogen bonding in the apramycin-ribosomal decoding A-site interaction. ChemMedChem. 2022;e202200486.
43. Verma AK, Chennaiah A, Dubbu S, Vankar YD. Palladium catalyzed synthesis of sugar-fused indolines via C(sp2)-H/N-H activation. Carbohydr Res. 2019;473:57-65.
44. Konidala SK, Kotra V, Danduga RCSR, Kola PK, Bhandare RR, Shaik AB, et al. Design, multistep synthesis and in-vitro antimicrobial and antioxidant screening of coumarin clubbed chalcone hybrids through molecular hybridization approach. Arab J Chem. 2021;14:103154.
45. Liu H, Sun D, Du H, Zheng C, Li J, Piao H, et al. Synthesis and biological evaluation of tryptophan-derived rhodanine derivatives as PTP1B inhibitors and anti-bacterial agents. Eur J Med Chem. 2019;172:163-73.
46. Konechnyi YT, Lozynskyi AV, Horishny VY, Konechna RT, Vynnytska RB, Korniychuk OP, et al. Synthesis of indoline-thiazolidinone hybrids with antibacterial and antifungal activities. Biopolym Cell. 2020;36:381-91.
47. Akunuri R, Unnissa T, Kaul G, Akhir A, Saxena D, Wajidali M, et al. Synthesis and antibacterial evaluation of rhodanine and its related heterocyclic compounds against S. aureus and A. baumannii. Chem Biodivers. 2022;19:e202200213.
48. Pardasavio PT, Pardasavi P, Sherry D, Chatarverdi V. Synthetic and antibacterial studies of rhodanine derivatives with indol-2,3-diones. Ind J Chem. 2001;40B:1275-8.
49. Song MX, Li SH, Peng JY, Guo TT, Xu WH, Xiong SF, et al. Synthesis and bioactivity evaluation of N-arylsulfonylindole analogs bearing a rhodanine moiety as antibacterial agents. Molecules. 2017;22:970.
50. Banerjee P, Eckert AO, Schrey AK, Preissner R. ProTox-II: A webserver for the prediction of toxicity of chemicals. Nucleic Acids Res. 2018;46:W257-W263.
51. Kritsi E, Matsoukas MT, Potamitis C, Detsi A, Ivanov M, Sokovic M, et al. Novel hit compounds as putative antifungals: The case of Aspergillus fumigatus. Molecules. 2019;24:3853.

52. Aleksić M, Stanisavljević D, Smiljković M, Vasiljević P, Stevanović M, Sokovic M, et al. Pyrimethanil: Between efficient fungicide against Aspergillus rot on cherry tomato and cytotoxic agent on human cell lines. Ann Appl Biol. 2019;175:228-35.
53. Fesatidou M, Zagaliotis P, Camoutsis C, Perou A, Eleftheriou P, Tratrtat C, et al. 5-Adamantan thiadiazole-based thiazolidinones as antimicrobial agents: Design, synthesis, molecular docking and evaluation. Bioorg Med Chem. 2018;26:4664-76.
54. Lipinski CA. Lead- and drug-like compounds: The rule-of-five revolution. Drug Discov Today Technol. 2004;1:337-41.
55. Sohlenius-Sternbeck AK, Terelius Y. Evaluation of ADMET Predictor in early discovery drug metabolism and pharmacokinetics project work. Drug Metab Dispos. 2022;50:95-104.
56. Naga D, Parrott N, Ecker GF, Morale AO. Evaluation of the success of high-throughput physiologically based pharmacokinetic (HT-PBPK) modeling predictions to inform early drug discovery. Mol Pharm. 2022;19:2203-16.
57. Kuriwaki I, Kameda M, Iikubo K, Hisamichi H, Kawamoto Y, Kikuchi S, et al. Discovery of ASP5878: Synthesis and structure–activity relationships of pyrimidine derivatives as pan-FGFRs inhibitors with improved metabolic stability and suppressed hERG channel inhibitory activity. Bioorg Med Chem. 2022;59:116657.
58. Tseligka ED, Rova A, Amanatiadou EP, Calabrese G, Tsibouklis J, Fatouros DG, et al. Pharmacological development of target-specific delocalized lipophilic cation-functionalized carboranes for cancer therapy. Pharm Res. 2016;33:1945-58.
59. Benson TE, Walsh CT, Massey V. Kinetic characterization of wild-type and S229A mutant MurB: Evidence for the role of Ser 229 as a general acid. Biochemistry. 1997;36:796-805.
60. Zhang J, He K, Cai L, Chen YC, Yang Y, Shi Q, et al. Inhibition of bile salt transport by drugs associated with liver injury in primary hepatocytes from human, monkey, dog, rat, and mouse. Chem Biol Interact. 2016;255:45-54.